REPORT DOCUMENTATION PAGE

Form Approved
OMB No. 0704-0188

1. REPORT DATE *(DD-MM-YYYY)*	2. REPORT TYPE	3. DATES COVERED *(From - To)*
19-11-2004	**Final Report**	**11 Feb 2003 to 11 Nov 2004**

4. TITLE AND SUBTITLE
Frictionless Linear Electrical Generator for Harvesting Motion Energy

5a. CONTRACT NUMBER
MDA972-03-C-0025

5b. GRANT NUMBER

5c. PROGRAM ELEMENT NUMBER

6. AUTHOR(S)
Jeffrey T. Cheung

5d. PROJECT NUMBER

5e. TASK NUMBER

5f. WORK UNIT NUMBER

7. PERFORMING ORGANIZATION NAME(S) AND ADDRESS(ES)
Rockwell Scientific Company LLC
1049 Camino Dos Rios, Thousand Oaks, CA 91360

8. PERFORMING ORGANIZATION REPORT NUMBER
71222

9. SPONSORING/MONITORING AGENCY NAME(S) AND ADDRESS(ES)
DARPA/Advanced Technology Office
3701 N. Fairfax Drive, Arlington, VA 22203-1714

10. SPONSOR/MONITOR'S ACRONYM(S)

11. SPONSOR/MONITOR'S REPORT NUMBER(S)

12. DISTRIBUTION/AVAILABILITY STATEMENT
Approved for public release; distribution unlimited.

13. SUPPLEMENTARY NOTES
The views, opinions and/or findings contained in this report are those of the author(s) and should not be construed as an official Department of the Army position, policy or decision, unless so designated by other documentation.

14. ABSTRACT

A key limitation in a buoy-based oceanographic monitoring system is the lack of a reliable power source with long operational lifetime. Battery packs suffer from the replacement cost and inconvenience. Traditional renewable energy devices do not fully address the need due to their poor performance in the hostile marine environment (e.g. solar cells) or size and cost (e.g. OWEC systems). To fill this important niche, we have developed a new technology that combines the uses of an ultra low friction surface treatment with an efficient linear generator. The small device can be deployed anywhere on the ocean surface without anchoring to the seabed. The friction between the sliding magnetic stacks and the inner wall of the generator is negligibly low. This not only reduces the frictional loss but also increases the system sensitivity to capture energy from the slightest movement. As magnets slide across induction coils in a tube, random AC outputs are produced. They are then rectified and regulated into stable DC output to charge a battery with an overall net efficiency of over 50% over a wide temperature range. Small prototype devices have been-field tested at near shore under mild wave conditions to produce close to 1 Watt of power and it can be scaled up to higher power capacity. The completely sealed structure makes the system corrosion resistant. The ultra low friction surface and simple design make the device mechanically robust without any sign of mechanical degradation after months of continuous operation.

15. SUBJECT TERMS

16. SECURITY CLASSIFICATION OF:			17. LIMITATION OF ABSTRACT	18. NUMBER OF PAGES	19a. NAME OF RESPONSIBLE PERSON
a. REPORT	b. ABSTRACT	c. THIS PAGE			19b. TELEPHONE NUMBER *(Include area code)*
Unclass	Unclass	Unclass	UL	43	

ROCKWELL SCIENTIFIC

SC71222.RFRFTV

Frictionless Linear Electrical Generator for Harvesting Motion Energy

Final Report for the Period: 2/11/2003 thru 11/11/2004

Submitted to:
DARPA/ATO: Dr. Edward M. Carapezza

Sponsored by
Defense Advanced Research Projects Agency
Advanced Technology Office (ATO)
ARPA Order No. P225/AD
Issued by DARPA/CMO Under
Contract No. MDA972-03-C-0025-CLN0001AB

Report Prepared and compiled by:
Jeffrey T. Cheung
Principal Investigator
Tel: 805.373.4144; jcheung@rwsc.com

Performing Organizations:
Rockwell Scientific Company
Scripps Institute of Oceanography

ROCKWELL SCIENTIFIC

SC71222.RFRFTV

Table of Contents

1.0 Introduction

In marine-based sensor buoy technology, the power source is an area that needs improvement in order to keep abreast with the development of the rest of the system. On most buoys, sensors and telemetry equipments rely on power from battery packs. They have a finite lifetime and require periodic replacements that are both costly and inconvenient, especially for systems deployed in remote regions. The increasing functionality and complexity of future marine instruments demand more power consumption over a longer operational lifetime, a need that can no longer be met by using batteries. Renewable energy sources such as solar and wind energy have been used on a limited basis. They are developed primarily as land-based technologies and are incompatible with the hostile marine environment. Their performance level varies with geographic, seasonal, and weather conditions. Survivability in the high-salinity environment and severe weather conditions also presents a challenge. Finally, solar panel and wind turbine require large buoy size and the tall structure makes them overt targets.

On the other hand, the ocean environment offers tremendous energy in the form of random wave motions. Their power spectrum depends on the sea state and the seabed topography but they are present at all times. Harvesting ocean power has been a subject of continuous development for more than a century. Nearly all projects are mammoth in scale and not suitable to be integrated to buoys. In this program, we developed a new type of wave energy harvester with a novel approach. It is robust and scaleable and can be fitted to small sensor buoys to convert the random wave motion into electrical energy. Though its operation is based on an extremely simple principle of passing magnets through a set of induction coils, its competitive edge comes from the enabling technology of an ultra low friction ferrofluid bearing that reduces the frictional loss, eliminates frictional wear and enhances system sensitivity to capture energy from the slightest amount of motion in all directions. We have understood the physics of ultra low friction behavior, improved its chemistry to extend its load behavior, and developed a family of energy harvesting generators based on guidance provided by modeling. The two types of generators are: Closed Tube Generator (single and multiple stack, parallel and orthogonal configuration), and Semi Closed Tube Generator with a point absorber (horizontal and vertical operation). Their performance will cover a broad spectrum of ocean wave conditions from near shore (where most energy is stored in horizontal wave propagation) to deep-sea applications (where most energy content is stored in the form of the slow yet powerful vertical motion of the waves). Based on our results, we will outline future objectives to continue this program to bring the technology to a next level ready for system insertion demonstration in a variety of oceanographic programs.

2.0 Ultra Low Friction and Ferrofluid bearings

2-1 Properties of the Ferrofluid

The friction between two solid surfaces depends on their chemical compatibility, local physical properties, and microstructures at the interface. The role of a lubricant is to fill part of the surface irregularities with a soft and low viscosity material to reduce the frictional restriction. Table 2.1 shows the static coefficient of friction μ_{static} between a 0.25" diameter, 0.5" long NdFeB magnet and various non-magnetic materials. When ferrofluid is applied to the magnet surface, the friction coefficient is reduced drastically by several orders of magnitude. This remarkable phenomenon forms the basis of the ultra low friction ferrofluid bearing that enables the level of performance of the power harvesting generators developed in this program.

Surface	μ_s
Nylon	0.33
Teflon	0.31
Polycarbonate	0.52
Glass	0.38
Ice/Ice at 0° C	0.02
Teflon/Teflon	0.05
Polycarbonate with Ferrofluid bearing	0.0008-0.0012

Table 2.1
Static coefficient of friction between NdFeB magnet and common non-magnetic materials

The static coefficient of friction of a NdFeB magnet with a ferrofluid bearing on a non-magnet surface was measured by placing a cylindrical magnet on its side in the V-groove of a non-magnetic test piece. The test piece was placed at the center of a 1.5-meter long aluminum beam with both ends secured to micrometers for fine height adjustment. The beam is oriented along the east-west direction in order to minimize the effect of the earth's magnetic field. A few drops of ferrofluid were applied to the magnet to engulf around its polar regions. After the beam was leveled completely, one end of the beam was slowly raised at 5-micron intervals until the inclination reached a critical angle when the magnet started to slide. The measurement was repeated by raising the other end. The average of the two values was used as the critical angle Θ_c. Static coefficient of friction was calculated as $\mu_s=\tan\Theta_c$. The results for different non-magnetic materials (aluminum, polycarbonate, Teflon and nylon), magnet sizes, and ferrofluid grades are independent of the non-magnetic material but strongly dependent on magnet size (Table 2.2a) and ferrofluid viscosity (Table 2.2b).

Table 2.2a: Static coefficient of friction of ferrofluid bearings on a 0.25" diameter 0.5" length magnet vs. viscosity of the ferrofluid

Magnet size (diameter x length)	μ_s
0.25"x0.25"	0.0008
0.5"x0.5"	0.0011
1"x1"	0.012
1.5"x1.8"	0.11

Table 2.2b: Static coefficient of friction of a 0.25" diameter 0.5" length NdFeB magnet on polycarbonate surface vs. viscosity of ferrofluid

Viscosity (cp)	μ_s
<1	0.0008-0.0012
4.2	0.005
7.2	0.016
300	0.02-0.04

The kinetic coefficient of friction was determined for a 0.25" diameter, 0.5" length magnet sliding inside a 1" I.D. glass tube placed on a known angle of inclination. Its velocity and acceleration were determined from the time-of-flight measurement made by three induction coils at 10 cm spacing. The dynamic coefficient of friction was calculated from these measurements. At a velocity of slower than 1 meter/second, the static and kinetic coefficients are comparable but at high velocity the kinetic coefficient is 20% higher and that is contrary to the traditional theory of friction. We attribute this anomaly to air resistance and the drag of ferrofluid. Experiments were conducted to understand the cause of the ultra low friction phenomenon and results showed that it depended on load (see Table 2.2a). From these findings, we developed solutions to overcome this limitation.

Ferrofluid is a homogeneous suspension of nano ferrite particles such as Fe_3O_4, and γ-Fe_2O_3 in various liquid carriers. These particles, approximately 10 nm in diameter, are covered with a layer of surfactant molecules, or ligands. As two particles approach each other due to Van der Wall's attraction, repulsion between the ligands keeps them from aggregating. When ferrofluid is applied to a magnet, the ferrite particles are attracted along the magnet flux lines and concentrate around the polar regions. Figure 2.1 shows the calculated flux distribution of a cylindrical magnet. The edges around the ends of the cylinder have the highest flux density and attract most ferrofluid. This is in good

agreement with the distribution of ferrofluid around a cylindrical magnet shown in Fig. 2.1b.

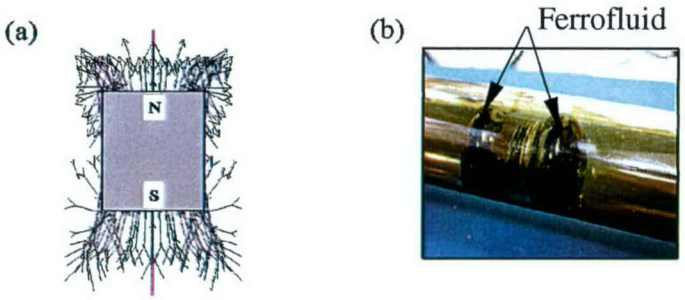

Fig. 2.1: A cylindrical engulfed by ferrofluid.

When a magnet is placed on a non-magnetic surface, the layer of ferrofluid serves as a cushion upon which the magnet glides over the surface without making direct contact. The frictional resistance comes solely from the shearing force of the liquid, which is determined by its viscosity. We have systematically tuned the viscosity of ferrofluid from less than one centipose (cp) to 300 centipose (measured by a Dynamic Mechanical Analyzer) by varying its concentration and liquid carrier. Due to the concentration difference, their magnetic permeability varies accordingly. The relationship between the friction (for a 0.25" diameter, 0.5" length magnet) and the ferrofluid viscosity is plotted in Fig. 2.2.

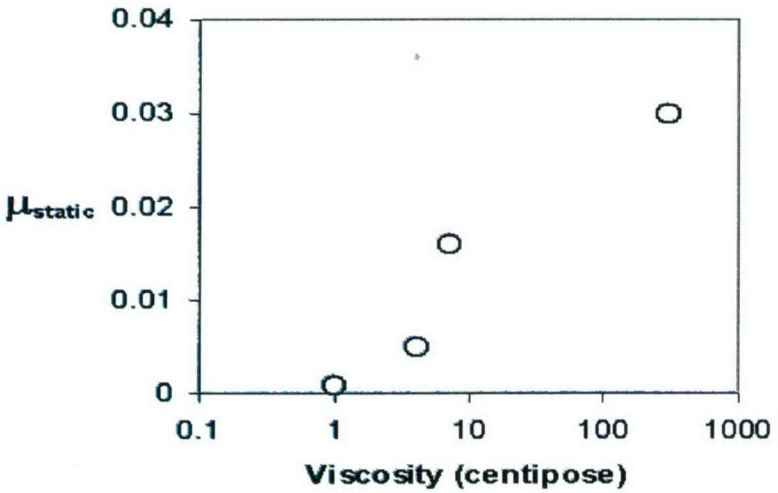

Figure 2.2: Static coefficient of friction of ferrofluid vs fluid viscosity

The highly nonlinear behavior differs from the classical description of fluid lubrication, which would predict a linear dependence. We believe this effect to be caused by the higher magnetic permeability of the more viscous ferrofluid samples. Their interaction with the field of the permanent magnet is stronger. Such interaction, as we learned later, can drastically change the rheological property of the fluid. Strong magnetic field induces magnetic nano particles to form semi-rigid long chains and slows their movement in the liquid carrier. Consequently, the viscosity and friction increase.

Results of the ferrofluid viscosity in the presence of a magnetic field are shown in Fig. 2.3.

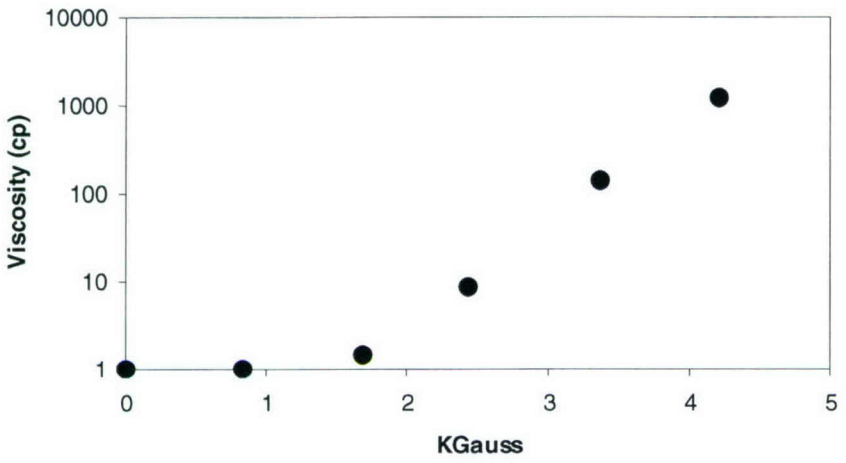

Fig. 2.3 Viscosity of ferrofluid vs. magnetic field strength

At a magnetic field strength of greater than 1 kiloGauss, the viscosity increases rapidly. The load dependence of friction coefficients shown in Table 2.2a can be explained by this effect. When a cylindrical magnet is placed on it side, it rests on the ferrofluid cushions that make point contact with the surface. As the magnet size (diameter and length) increases, the total weight increases with the volume while the contact areas under the ferrofluid cushions only increase linearly. Therefore, pressure on the ferrofluid cushion increases quadratically with the magnet size. For a large magnet, the ferrofluid is compressed to a very thin layer and is close to the magnet surface where the field is the most intense. This friction increases accordingly as shown in Fig. 2.4.

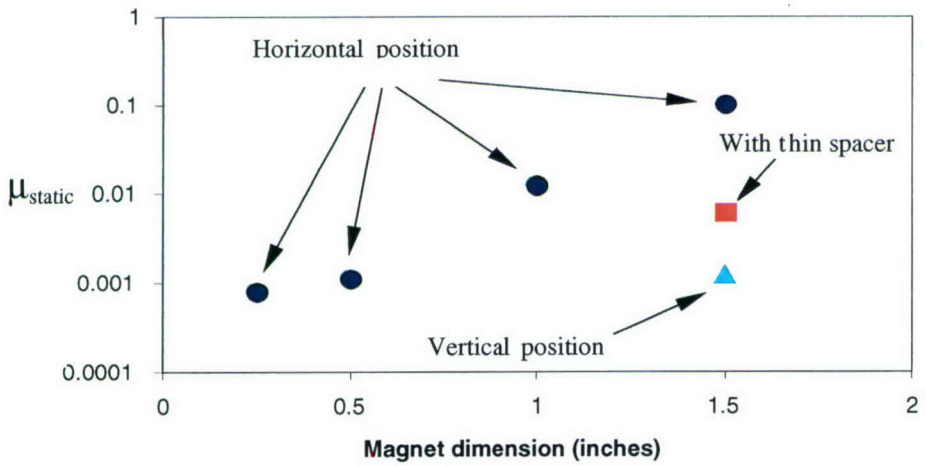

Figure 2.4: Static coefficients vs. magnet dimension (diameter=length)

The increase in friction caused by a large load poses a dilemma to the development of a wave energy harvester, which needs large magnets to generate more power. There are several solutions. The first solution is to replace a single generator with large magnets

with an array of smaller generators. This approach increases the system complexity, especially the energy harvesting and conditioning circuitry. The second solution is to change the geometry of the generator. A simple approach is to separate two magnets of opposing polarity with a thin spacer made of a magnetic material such as low carbon steel. This will create a zone at the center of the spacer where the magnet field is very weak due to field cancellation. Ferrofluid tends to concentrate at the corner of the two magnets. If the spacer is thin enough, the two separate ferrofluid bearings will fuse together to form a continuous cushion by surface tension. The center portion on which the ferrofluid rests has much lower friction due to flux cancellation of two magnets. For 1.5" diameter, 1.8" length magnets with a 0.25" thick spacing, this simple approach can reduce the friction by more than one order of magnitude from 0.1 to 0.007 (See figure 2.4) We chose to apply this simple approach for linear generators. Another solution is to develop a linear generator where the magnetic axis is orthogonal to the sliding motion. In this configuration, the magnets will slide on a large ferrofluid cushion covering its entire cross section area at the end. The cushion is much thicker and the friction for a 1.5" diameter 2" length magnet is as low as 0.001 (See figure 2.4). This design is more complex but will have better performance. We propose to develop this generator as the platform for more powerful and adaptive generators in the next phase work of this program.

2-2 Effect of Ultra Low Friction on Generator Performance

The basic device is a linear electrical generator shown in Fig. 2.5. A cylindrical magnet or magnetic stack with ferrofluid bearing is placed inside a tube with its magnetic axis parallel to the tube. To leave an air passage gap the diameter of the ferrofluid bearing is slightly smaller than the I.D. of the tube. Under nominal operation, the effect of air resistance is negligible. Small magnets mounted on both ends of the tube are oriented with their polar axis opposing that of the moving magnet to provide recoil. Because of the high coercive field of the NdFeB magnets, recoil collisions from the end are nearly elastic. Induction coils are wrapped around the tube to capture electrical current generated in the coil as the magnet passes through it. The voltage (V), the magnet cross section (A), the rate of flux change ($d\Phi/dt$) across the coil of N turns, and the average power (P) captured by the load resistor R_L are related by the Lenz Law as follows:

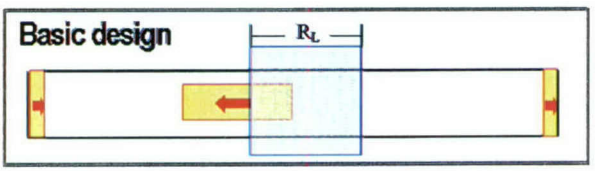

$$V(t) = NA\, d\Phi/dt$$

$$P(t) = V^2 / R_L$$

$$< P >= \frac{\int_{t_1}^{t_2} P(t)dt}{t_2 - t_1}$$

Fig. 2.5: Schematic of a linear generator

The use of ultra low friction ferrofluid bearings drastically improves its performance. It reduces frictional loss, eliminates friction wear, increases system

sensitivity and gives design freedom to incorporate features that are otherwise impossible.

2.2.1 Low frictional loss and high device sensitivity

We carried out modeling calculations to study the effect of friction on energy conversion efficiency. Fig. 2.6 shows the calculation of the effect of friction coefficient on the relative energy conversion efficiency of a linear generator as a magnet slides down from two different angles of inclination. Good agreement was found between the model calculation and experimental data. The results clearly indicate the advantage of ferrofluid bearing especially for small angle of inclination. In this device configuration, the magnet makes only one pass through the coil in every period. In a multiple magnet generator, the magnet movement is chaotic, with multiple collisions within the same period of external excitation. Frictional loss will have a cumulative effect, and therefore, the significance of the ultra low friction bearing is more amplified in a multiple magnet generator.

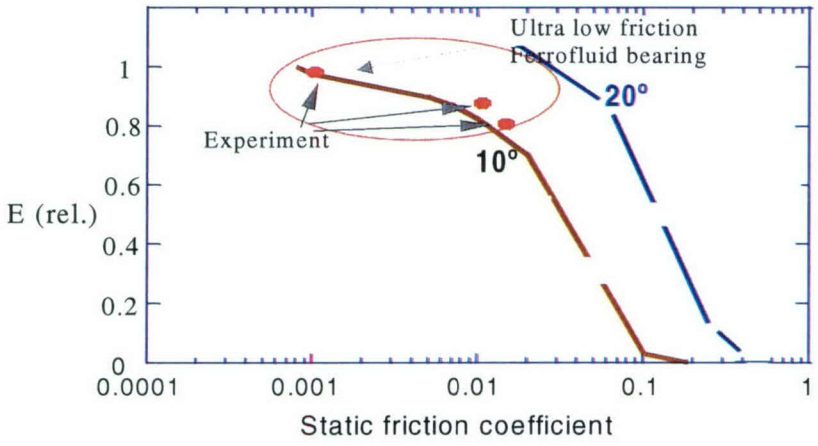

Figure 2.6: Effect of friction on relative energy output

The advantage of using Ferrofluid over regular lubricant such as WD-40 oil was also verified by comparing the power output from a large generator consisting of a stack of alternating 1" magnets at 26° inclination with WD-40 lubricant and with Ferrofluid bearing. The generator with Ferrofluid lubricant delivers more than a 4-fold increase over the use of WD-lubricant. Of course, as the inclination angle decreases, the improvement becomes even larger.

2.2.2 Temperature dependence

The temperature dependence of energy harvesting efficiency was measured by immersing a generator in a constant temperature bath from subzero minus 10°C to a tropical 40°C. This temperature range is well below the Curie point of the NdFeB magnet therefore the effect is caused by the change of Ferrofluid viscosity. Results are shown in

Fig. 2.7. By properly reformulating the liquid carrier, we minimized its viscosity change at very low temperature. With this new formulation, the capture efficiency shows only a less than 10% decline over the entire temperature range.

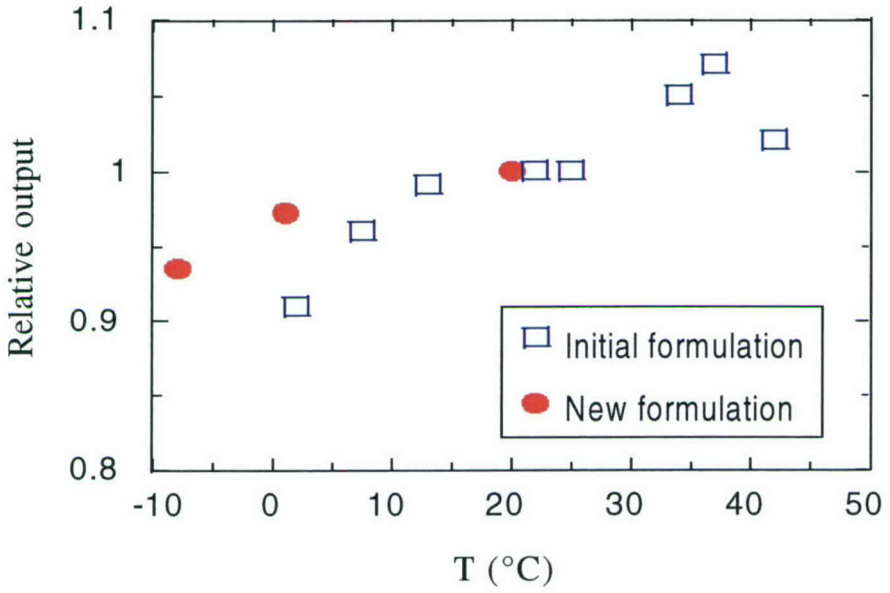

Figure 2.7: Temperature dependence

2.2.3 Robustness

A test was performed to address two reliability issues: frictional wear and the long-term stability of the ferrofluid over a long-term agitation. A small single magnet generator was placed on a mechanical shaker at 2 Hz. Because of the interaction with the end recoil magnets, every cycle would induce 5 rapid oscillations of 0.7 cm amplitude. Its electrical output was monitored periodically. After more than four months of continuous operation of more than 4×10^7 oscillations, there was no sign of degradation (Fig. 2.8).

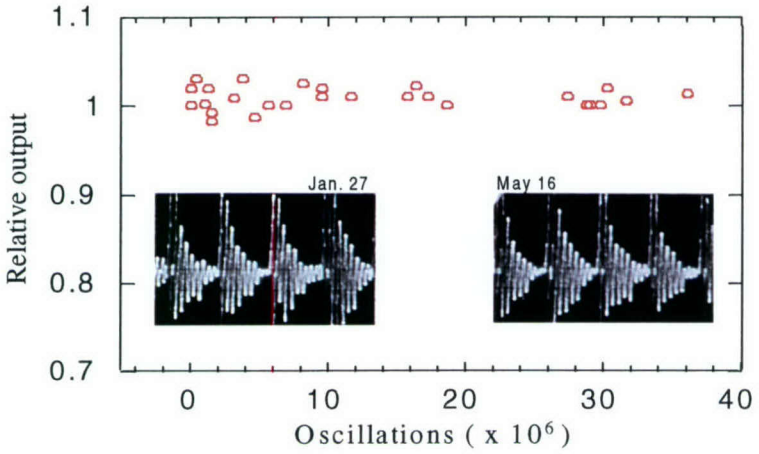

Figure 2.8: Long-term stability tests

3.0 Generator Developments and Testing

Throughout this program, we have established a deep understanding in the design and performance of linear generators with ferrofluid bearings. Theoretical modeling tools were developed to guide the experimental work and predict generator performance. During the program, the basic single stack close tube generator evolved into some more elaborate configurations such as a *multiple stack close tube generator*, and a *semi open generator with a point absorber* for both horizontal and vertical operation. These new generators are more powerful, and efficient. They are also more adaptable to a wide range of sea states.

3-1 Theoretical modeling

3.1.1 Equation of motion, electro-mechanical modeling

The theoretical model that we routinely use to aid generator design is an RSC developed Electro-Mechanical Model that solves the equation of motion of a magnet in the dynamic system. All interaction forces are accounted for. For computational convenience, each magnet is assumed to be a single point dipole with the strength of a grade 32 NdFeB magnet. The validity of this assumption was confirmed to be within 15% error of the exact calculations by the much more elaborate numerical computational routine involving complex volume integrals. For a single magnet generator, the equation can be expressed by equating the force acting on the magnet as the sum of five types of forces shown in the following:

$$m\frac{d^2x}{dt^2} = \vec{F}_{end1}(x) + \vec{F}_{end2}(x) + \vec{F}_{coil}(x,t) + \vec{F}_{ext}(t) - F_{friction} \qquad (1)$$

where F_{end1} and F_{end2} are the interactions with end magnets 1 and 2, respectively. F_{coil} describes the interaction with counter EMF exerted by the induction coil as the magnet passes through. F_{ext} represents the external force coupled into the system to move the magnet. $F_{friction}$ is the frictional resistance force, a constant that is determined by the mass of the magnet and the its friction moving inside the tube. In a system that uses ferrofluid bearings, this term becomes negligible. For a multiple segment- single stack generator, each of the first three terms is replaced by summing the contributions from individual segments. The equation of motion is solved numerically by finite element analysis. Fig. 3.1 gives an example of the calculated trajectory of a 0.375" diameter, 7" total length multiple segment magnet stack oscillating between a pair of 0.5" diameter 0.125" thick end magnets in a 14" long tube. External force has a sinusoidal form to simulate the rocking motion. An induction coil with width matching the length of the individual magnet segment is placed in the center of the tube to record the motion of the magnet. The stack moves periodically as expected. The unexpected features are the three rapid oscillations with much smaller amplitude when the stack reaches near the end of the tube. These fine features were reproducible in the real operation with good agreement in frequency and amplitude, thus validating the model.

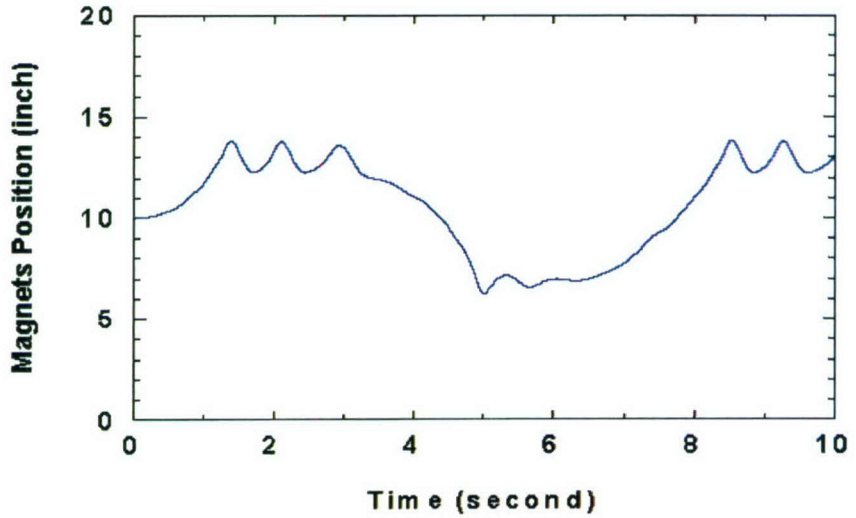

Figure 3.1: Trajectory calculation of an oscillating magnet in a single stack magnet system

After the equation of motion is solved, the velocity of the magnet can be calculated as it passes through the coil, as well as the induced voltage and the amount of electrical energy captured. We have used this model to predict the power output as a function of tube length, magnet size, recoil magnet strength and other design features with great success.

This model has also been extended to solve the magnet motion in a two -magnet system by setting up a pair of coupled differential equations. They are similar to equation (1) with an additional term $F_{1\text{-}2}$ to account for the interaction between the moving magnets:

$$m\frac{d^2x_1}{dt^2} = \vec{F}_{end1\text{-}1}(x_1) + \vec{F}_{end2\text{-}1}(x_1) + \vec{F}_{1\text{-}2}(x_1) + \vec{F}_{coil}(x_1,t) + \vec{F}_{ext}(t) - F_{friction}$$
$$m\frac{d^2x_2}{dt^2} = \vec{F}_{end1\text{-}2}(x_2) + \vec{F}_{end2\text{-}2}(x_2) + \vec{F}_{1\text{-}2}(x_2) + \vec{F}_{coil}(x_2,t) + \vec{F}_{ext}(t) - F_{friction} \quad (2)$$

For simplicity, we omitted $F_{coil}(x_1, t)$ and $F_{coil}(x_2,t)$ terms to calculate the magnet moving trajectory in the absence of a counter EMF. Other conditions were the same as the calculation for the 1 magnet system. A power output calculation for a double magnet generator is shown in Fig. 3.2.

Compared to the single magnet system, the trajectory is much more complex with multiple frequency components. Again, the modeling calculation is in good agreement with experimental observation. The complex movement arises from the close coupling between the two moving magnets and two end magnets, resulting in a near chaotic situation. It enhances the sensitivity to interact with external excitation, and increases power harvesting efficiency.

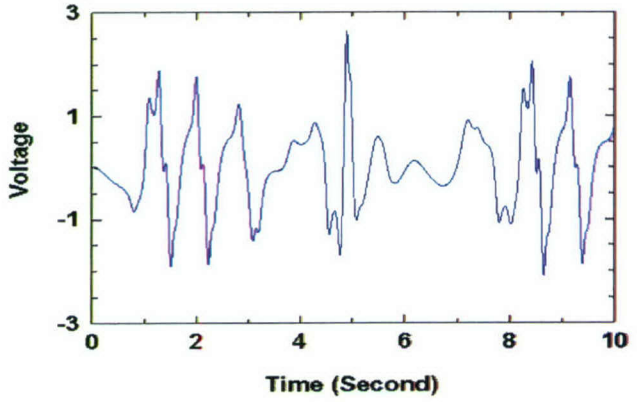

Figure 3.2: Trajectory calculation of an oscillating magnet in a double magnet system

3.1.2 Magnetic flux management modeling

Since the induced voltage is proportional to the square of the rate of flux change inside the coil, it is important to maximize the field gradient along the polar axis of a cylindrical magnet as it travels through a coil in the same direction. A simple single magnet linear generator shown in Fig. 2.5 behaves poorly in this aspect because of flux loss in the fringe field and the leakage through the finite air gap. By extensive modeling of the magnet flux distribution in various geometric arrangements, we found two solutions. Modeling computation was performed with a commercial software MagNet™

(Infolytica Inc.) that provides both static and dynamic modeling of magnetic flux distribution and its interaction with induction coils.

(1) Fringe field loss at the end of a cylindrical magnet

Figure 3.3 shows the flux distribution of a single cylindrical magnet and the amount of flux trapped by an induction coil as the magnet passes through. The fringe field penetrates deep into the region inside the coil before the magnet enters, therefore reducing the net change of flux density. The amounts of flux (in relative units) captured are 0.0088 and 0.0349 for a time period while the magnet is outside and inside of the coils, respectively, giving a net change of 0.0261 units.

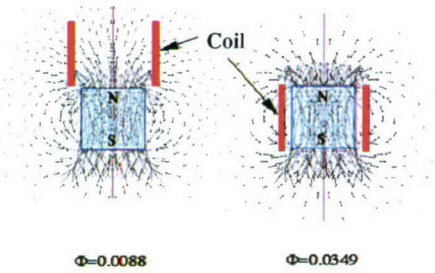

Figure 3.3: Fringe field loss at the end of a single magnet

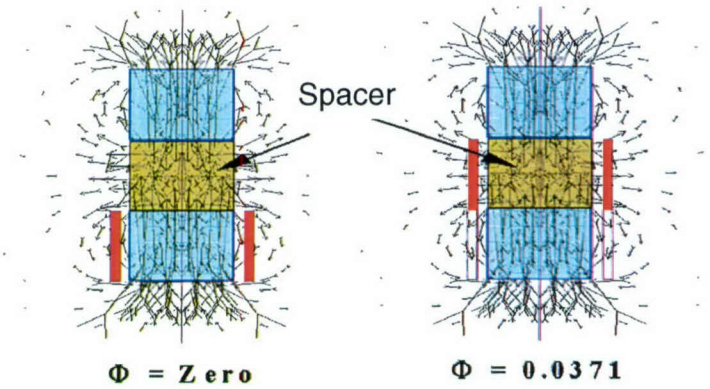

Figure 3.4: Magnetic flux captured by a coil from a moving two-segment magnet stack

The net amount of flux to be captured can be increased by stacking magnets along the magnetic axis with opposing polarity separated by thin spacers made of a magnetic material such as low carbon steel as in Fig. 3.4. The net flux in the center of the region between the two magnets is ZERO because of the complete cancellation from the two opposing magnets. The flux inside the magnet increases slightly to 0.0371 units. As a result, the flux change capture by the coil is 0.0371 units, a 40% improvement over the single magnet case. For the same velocity, the captured electrical energy is quadratically proportional to the net flux change, therefore will result in a 170% increase in the amount of energy harvested.

We measured this effect on the induced voltage output by passing a pair of magnets with opposing polarity through a coil while varying the thickness of the spacer. Results, plotted as V^2 vs. time, are shown in figure 3.5. The area under the curve is proportional to the amount of captured energy.

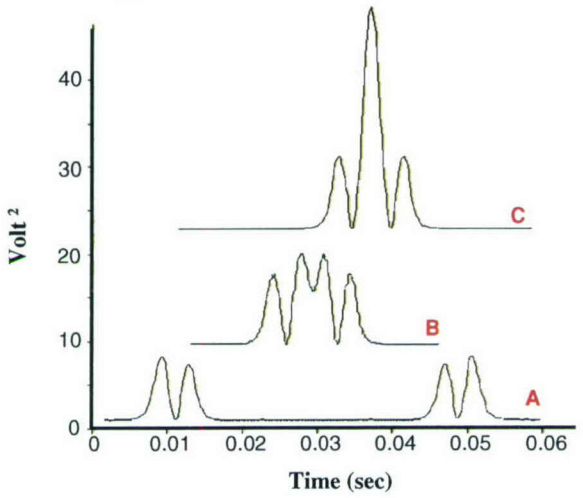

Figure 3.5: Amount of captured energy (i.e. the area under the curve) vs spacer thickness for a two-magnet stack

At large separation (case A), flux cancellation did not take place due to the short ranged magnetic potential, the behavior was just the sum of two isolated single magnets. As the separation decreased (cases B and C), the flux cancellation effect became more prominent and the amount of captured energy increased accordingly to reach a maximum at a gap of about 1/3 of the magnet length. The captured energy in this case increased by 60%. However, the two side peaks remained nearly unchanged because of the end effect. As the number of magnet segments in the stack increases, the relative amount of end effect will decrease proportionally. We measured that for stack with 10 magnet segments, the overall increase in captured energy was more than doubled over if single magnets were used.

(2) Flux leakage in the finite air gap

In an electrical generator, the air gap between the magnet and the coil must be kept to a minimum to reduce the flux leakage due to premature return inside the coil. In a linear generator with ferrofluid bearing, due to the large gap space to accommodate both the ferrofluid bearings and the air passage, a substantial amount of flux will return along a path inside of the coil shown in Fig. 3.6a. These returning fluxes cancel part of the flux inside the magnet so the net amount of flux captured by the coil is reduced. A simple solution is to cover the coil with a high permeability shield. This shield acts as a low reluctance path outside the coil for the returning fluxes shown in Fig. 3.6b. Consequently, the amount of net captured flux increases.

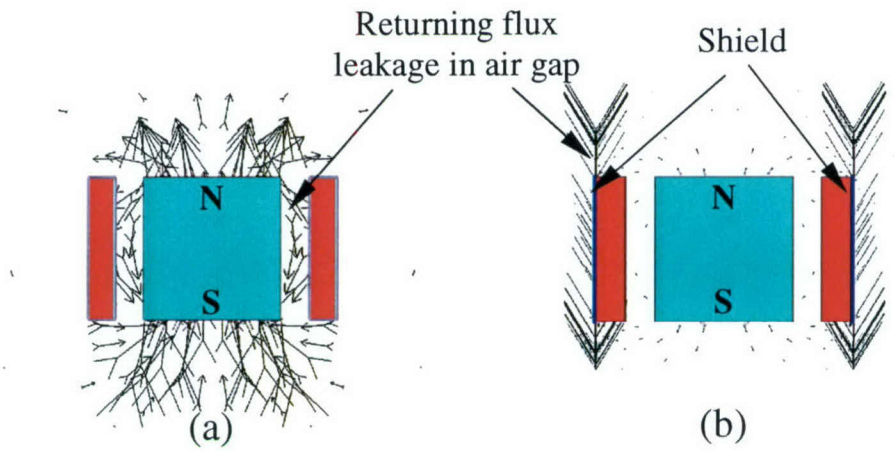

Figure 3.6: Effect of high permeability shield on reducing the air gap leakage (a) without shield, (b) with shield

We also calculated the effectiveness on thickness and permeability. Results show that the use of 0.004" thick high permeability foil (μ=4000) is sufficient. For an air gap of 0.2" that is required for the ferrofluid bearing, this shield will increase flux capture by 12% or 25% more if the velocity is kept constant.

3-2 Electronic Circuit Design

3.2.1 Circuit for single magnet stack generator

An energy harvesting circuit converts random AC power from the coils to regulated DC output suitable for charging batteries. At the same time, it controls the timing and magnitude of the counter EMF to ensure smooth magnet movement, and efficient energy capture/conversion.

We have developed a circuit to meet these performance criteria. The circuit, shown in Fig. 3.7, consists of four parts. Part A is a rectifier bridge made of low insertion loss Schottky diodes. The rectified output will charge a capacitor bank (B) until a preset voltage V_H is reached. At that point, the capacitors will be discharged to the power conditioning circuit (C) to convert it to a regulated DC output level suitable for charging the battery. During this cycle, the voltage across the capacitor decreases and the magnet is slowed down by the counter EMF. When the capacitor voltage reaches the second preset level V_L, the circuit will switch back to the charging mode and the magnet stack movement will pick up again. The conversion efficiency of this quasi-continuous circuit is 75-80%. Half of the loss arises from the diodes in the rectifier bridge. A multiple number of this circuit can be used in parallel to simultaneously process the output of discrete generators and combine their output to a single source. This circuit has been tested successfully for over two weeks of continuous operation to harvest energy from a

generator under rocking motion and produce stable DC power to charge a lead acid battery.

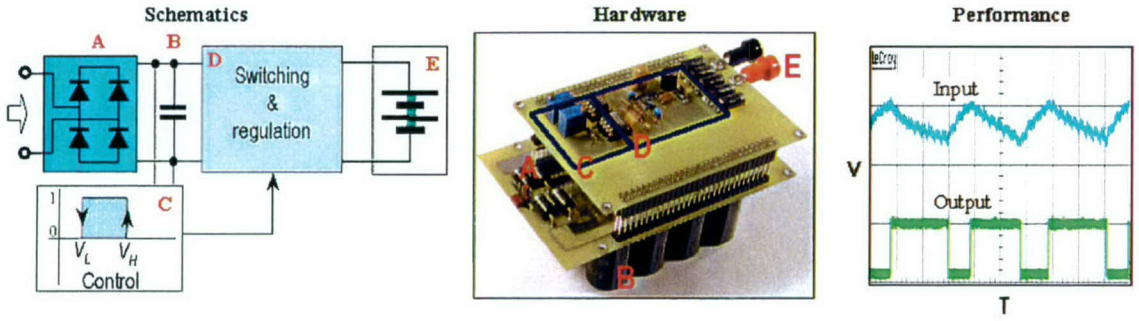

Figure 3.7: Power harvesting/regulating circuit

3.2.2 A Dynamic Distributive Circuit for Multiple Stack Devices

We have shown in model simulation and later verified experimentally that a multiple stack generator is more effective than a single stack generator in coupling external excitation into the system. However, the output power from such a generator presents a challenge, since the outputs from different coils are out of phase and have random magnitude. Although a discrete circuit for each coil can be used to produce a steady DC output and combine the outputs, the approach is costly and ineffective. A dynamic distributive circuit has been developed to address this problem.

The solution is shown in Fig. 3.8 for a two-coil/multiple magnet system, but can be used for a multiple coil system. The AC output from each coil is connected to a rectifier bridge. Outputs from various rectifier bridges are then connected in PARALLEL to a common load R_L.

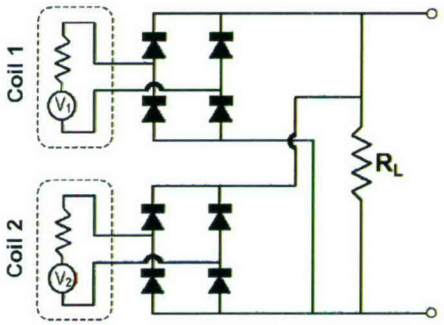

Figure 3.7: Parallel connection of rectified output from two coils

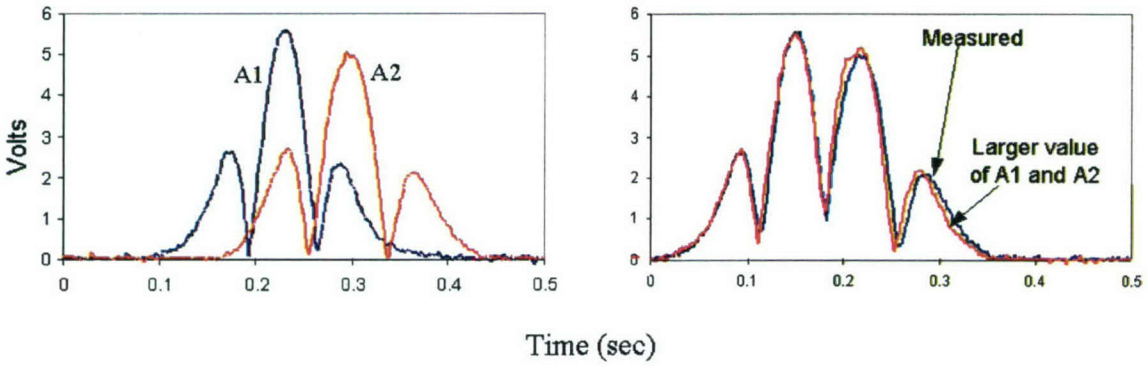

Figure 3.8: (a) Rectified output from two coils A1 and A2. (b) Rectified output of two coils connected in parallel, and comparison with the output by taking the higher voltage output of the two coils

Fig. 3.8 shows that the rectified outputs from two coils are out of phase. However, when they are connected in parallel to a common load resistor R_L, the circuit constantly reconfigures itself such that it only accepts the one with higher voltage, while the conductive of the other rectifier bridge is blocked. This switching action takes place continuously. Consequently, the net output is a superposition of the highest output. In other words, only one magnet is actively generating energy as a "Working Magnet". The other magnet moves freely in the absence of counter EM force since the coil is open. But it can transfer its energy to the "Working Magnet" via collision. The roles of these two magnets are interchangeable and can reverse at any instant depending on their output voltages. The dynamic distributive approach can be extended to a system with multiple moving magnets and multiple induction coils.

We have tested this circuit on a generator consisting of 5 magnets and 10 coils. Rectified outputs from individual coils were combined in parallel across a 14-Ohm load resistor as shown in Fig. 3.9. The generator was subjected to horizontal excitation at 0.5 Hz. The output power was measured as a function of the number of connecting coils.

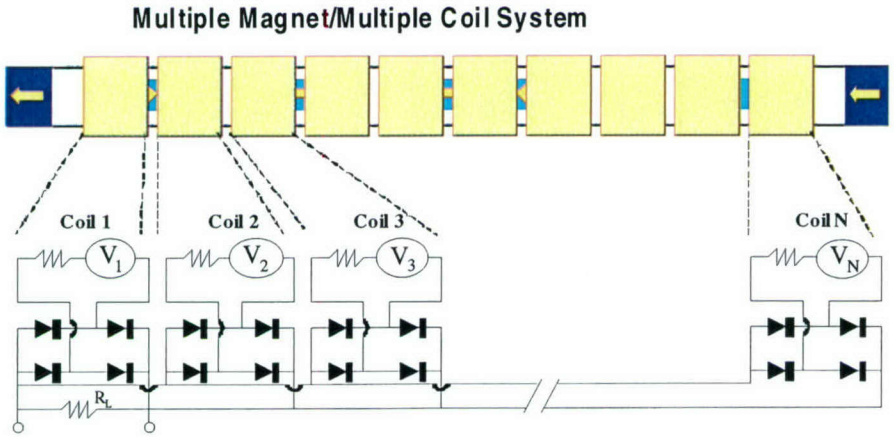

Figure 3.9: Schematic of a multiple magnet multiple coil generator connected to a rectifier bridge network.

Fig. 3.10 shows the output from a different number of coils. The rectified output shows very random peaks due to the strong coupling between the multiple magnets. As the number of coils increase, the circuit only switches on to capture the energy from the coil with the highest voltage outputs that merge to form a broadband DC output. The total output power scales linearly with the number of coils that locate near the center. The side coils, however, have little effect since their output voltage is always lower and therefore remain inactive.

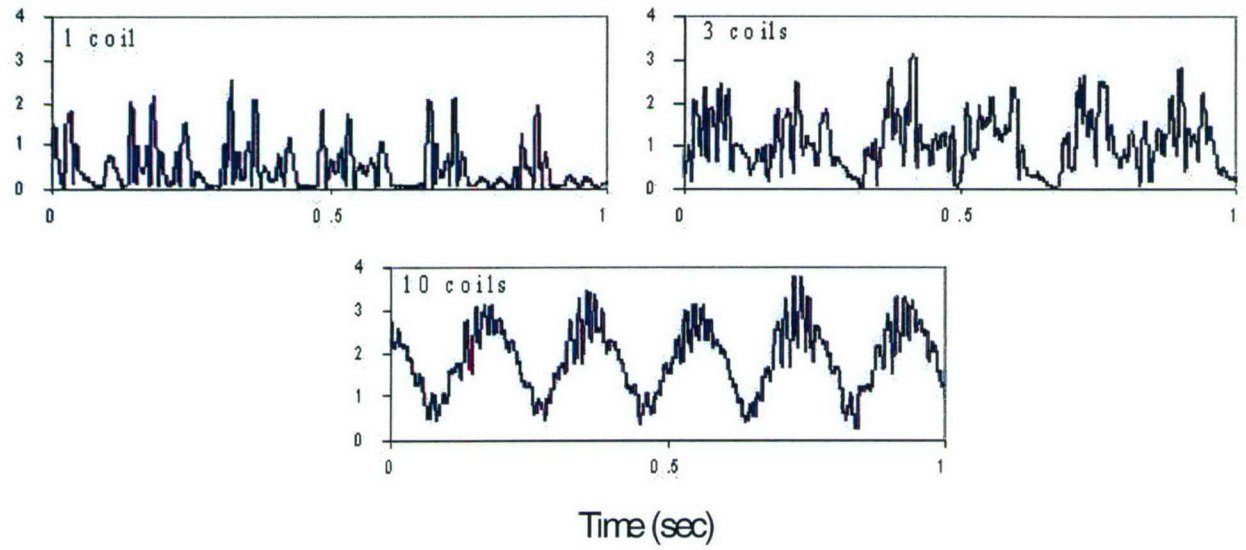

Fig. 3.10: Voltage output of a multiple magnet, multiple coil generator using the dynamic distributive circuit.

4.0 Surface Wave Energy Harvesting Generator Performance

We applied these basic tools and knowledge for designing the linear electrical generator to develop scale-up generators for testing. The energy flow from ocean waves to regulated DC output can be divided into four stages.

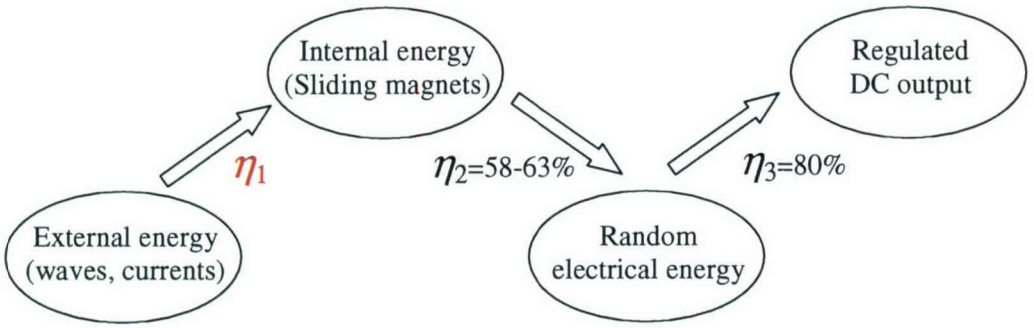

Figure 4.1: Steps to converting ocean wave energy to regulated DC power

The overall efficiency of energy conversion is the combined efficiency of three processes as in $\eta = \eta_1 \times \eta_2 \times \eta_3$. Among them, η_3 has been determined to be 80% based on our energy harvesting circuit and η_2 is approximately 60% for a multiple segment single stack generator. η_1 is difficult to quantify, because it varies with the nature of excitation energy, how it is coupled to the linear generator and the total mass of the buoy.

In this program, we developed two types of generators: (1) Closed Tube Generator (single and multiple-stack), and (2) Point Absorber Generator (horizontal and vertical configuration). All are capable of producing around 1 watt or higher power under nominal excitation. They share the same core technology of a linear generator with ultra low ferrofluid bearings, but they have different energy coupling mechanisms. The Closed Tube Generator uses an indirect coupling mechanism via recoil magnets on both ends and the Point Absorber Generator uses a direct coupling mechanism with a point absorber on one side. Design and performance details are described in the following sections.

4-1 Closed Tube Generator

This is the most basic design. The magnet stack(s) is placed inside a sealed tube with recoil magnets on both ends. The center portion of the tube is covered with coils with width and spacing matching the dimension of the magnet stack. Based on model computation, NdFeB magnets with near unity aspect ratio (i.e. length/diameter) gave the best performance in terms of minimum resistive loss in the coil and maximum flux per unit volume. They were stacked with their polar axes in alternating directions. Each segment is separated from its adjacent units by low carbon steel spacers about 20% of the thickness of each magnet segment. Low viscosity ferrofluid bearings were applied to the stack as shown in Fig. 4.2.

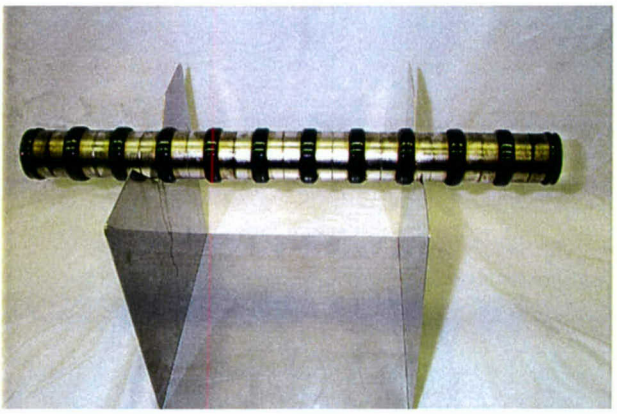

Figure 4.2: A magnetic stack with ferrofluid bearings

The magnet stack with Ferrofluid bearings is then sealed in a plastic tube. Four coil segments were wrapped around the tube and then covered with two layers of 0.002" thick high permeability metal foil for shielding to enhance the flux capture. To minimize the resistive loss in the unused coils, we chose the total length of the magnet stack to be 2/3 of the tube length, and the coil length to be 1/3 of the tube length. In this arrangement, there is always a voltage from each coil at any time of the operation regardless of the position of the magnetic stack. All outputs are in phase and can be combined by serial connection. A typical rectified output voltage from such a generator under 1 Hz external excitation is shown in Fig. 4.3.

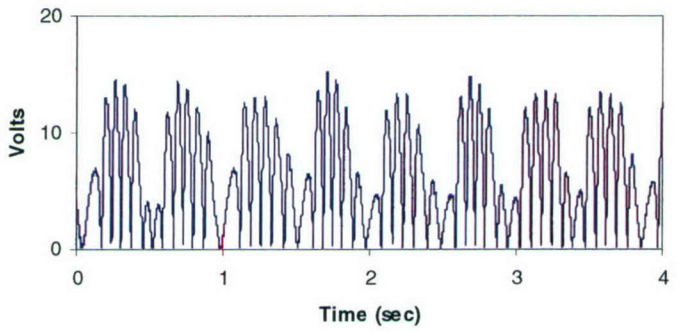

Figure 4.3: Typical rectified output from a generator with long magnet stack under rocking motion (device # 120904-3)

When placed horizontally, there are only two ways to couple external excitation energy into the Closed Tube Generator. One is *Horizontal Axial Excitation*, and the other *Vertical Rocking Excitation*. Both mechanisms were characterized for their advantages, disadvantages and limitations. Coupling efficiency η_1 was measured under various excitation conditions. Fig. 4.4 is a picture of the generator that was tested. The single stack is made of 8 segments of 1" diameter 1.25" long NdFeB magnets. Four spatially matched coils are around the center portion of tube and they are connected in series with

a total resistance of 50 Ohms. The coils are wrapped with a high permeability shield. A pair of 1" diameter, 0.25" thick magnets of the same grade are used as recoil magnets. The weight of the magnet stack is 40% of the entire generator.

Figure 4.4: Photograph of linear generator on a leaf spring support stand. Sideway movement of the vertical supports induces a horizontal axial excitation mode.

4.1.1 Axial excitation in horizontal position

The generator was placed on a holder that acted as a leaf spring (Fig. 4.4). We calibrated the spring constant for different materials (e.g. beryllium copper, stainless steel and fiber glass) and thickness.

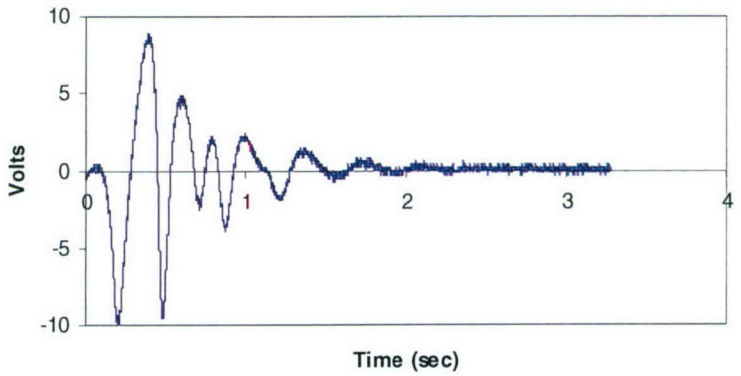

Figure 4.5: Voltage output across a resistive load after a single pulse axial excitation

The initial displacement was monitored by measuring the position of a laser beam reflected from the bending surface. By changing the amount of the initial displacement and spring constant, we were able to measure the acceleration and energy content of an excitation pulse used to drive the generator. The electrical energy captured was determined from the voltage output across a resistive load shown in Fig. 4.5. The leaf

spring has a low Q-factor and came to a complete stop after only one oscillation. However, the oscillation of the magnetic stack persisted for several periods. Fig. 4.6 shows the output electrical power vs. the load resistance after axial excitation by a pulse with 2.4 m/sec^2 initial acceleration and 1.12 Joule total energy.

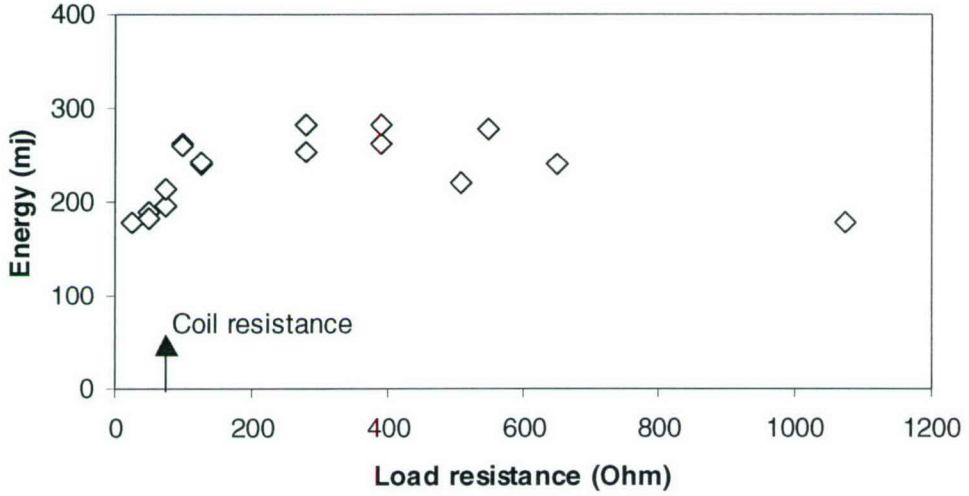

Figure 4.6: Captured electrical energy vs. load resistance

For a small load resistance, most of the induced current is petitioned into the coil, giving rise to resistive loss and a large counter EMF but small energy captured by the load. For very large load, the small counter EMF is small due to the low induction current. As a result, the amount of captured energy is also lower. In a broad maximum between load resistance of 150 Ohm-500 Ohm, the captured energy is about 270 mj, corresponding to 24% efficiency for coupling external energy into random electrical energy captured by the load resistor. This is the combined efficiency of η_1 and η_2 that can be expressed as $(\eta_1 \times \eta_2)$. Since the efficiency for converting energy from a moving magnet to random AC captured by the load resistor is 58-63% (i. e. η_2 in Fig. 4.1), we deduce that the efficiency for coupling external energy to the motion energy of the magnet (i.e. η_1) is about 40% under the above excitation condition. Most of the other 60% of energy was wasted in moving the entire generator (magnet, tube and coils) together without causing any relative motion between the two, and a small amount was dissipated in the leaf spring. This petition of total energy is consistent with the weight ratio of the magnet and the rest of the generator. Therefore, one way to further increase the efficiency η_1 is to increase the weight of the magnet stack and reduce the weight of the rest of the generator.

We have also measured the dependence of combined efficiency $(\eta_1 \times \eta_2)$ on the initial acceleration of the axial excitation while keeping the total energy content constant within 15% (Fig. 4.7).

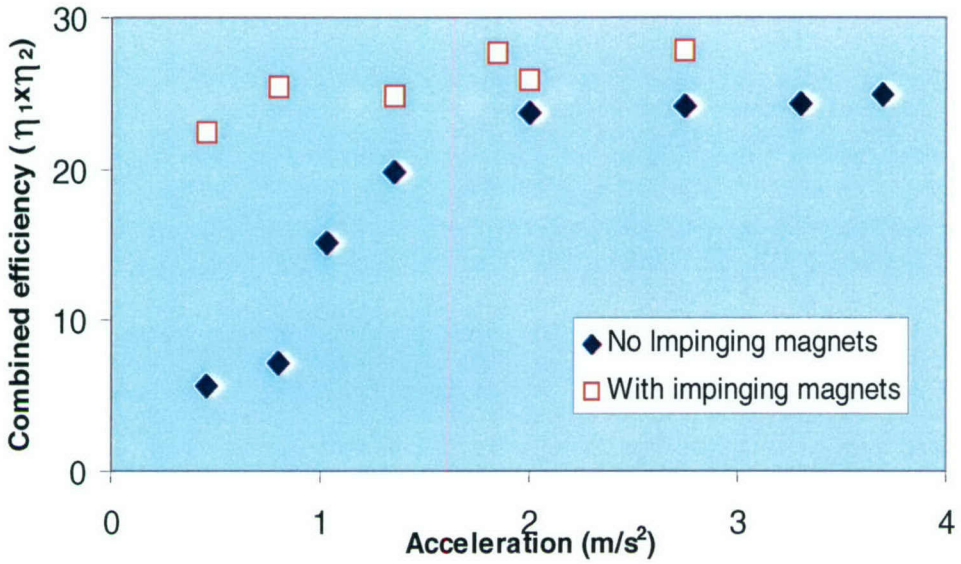

Figure 4.7: Combined efficiency ($\eta_1 x \eta_2$) vs. initial acceleration of the excitation pulse

The efficiency approaches a constant level at high acceleration, decreases with reduced acceleration and intercepts at zero. This can be interpreted by considering the excitation and energy production as a two-step process. At first, as the generator is pushed horizontally by initial excitation, the magnet stack tends to remain in place due to the low friction ferrofluid bearing, therefore creating a relative movement between the magnet and the coil. The movement produces an induction current in the coil and counter EMF that will impede the motion of the magnet. A strong acceleration provides the magnet stack with sufficient energy not just to overcome counter EMF but also to make a few oscillations as depicted in Fig. 4.5 before dissipating its energy into the coil. However, if the initial acceleration is small, the magnet does not have sufficient energy to overcome the counter EMF and will stop. At that point, the counter EMF vanishes, but the remaining portion of the first excitation pulse has already been dissipated as wasteful energy. We also made a few measurements by adding extra weights onto the generator. The extra weight lowered the amount of captured energy proportionally as the extra mass damped the spring action. Therefore, in the high acceleration limit of horizontal excitation of a closed tube single magnet generator, the combined energy transfer efficiency can be estimated as:

$$(\eta_1 \times \eta_2) \cong 0.6 \times (\boldsymbol{M}_{magnet} / \boldsymbol{M}_{total}) \qquad (3)$$

Where $\boldsymbol{M}_{magnet}$ and $\boldsymbol{M}_{total}$ are the mass of the magnet stack and the generator, respectively. If the generator is secured on a buoy, then $\boldsymbol{M}_{total}$ is the total mass of the entire system.

The amount of power captured by the resistive load averaged over a time interval is:

$$P_{Captured} \cong \frac{0.6 \times F \times (M_{Magnet} / M_{Total}) \times \phi \times \int_{t_0}^{t_1} E_{Excitation}(t)dt}{(t_1 - t_0)} \qquad (4)$$

where F is the frequency of the axial excitation pulses during the time interval (t_0-t_1), and ϕ is the relative phase of the motion of the magnet and the excitation force. If excitation is applied to the system in resonance with the phase of magnet movement, the efficiency will be at maximum, and vice versa as the two are out of phase. This condition is very difficult to achieve with a single stack generator. In addition to the significance of phase matching, the above shows that to have a large power production, the magnet stack must be as heavy possible with respect to the rest of the system, and the excitation force must have a high frequency. *Since most of the energy content in the ocean wave spectrum is slow and powerful motion, the use of single stack Closed Tube Generator to capture this type of energy is inefficient.*

The performance limitation under low acceleration excitation can be improved by a "3-Stack Generator" as shown in Fig. 4.8. The magnet stack in the middle is the "Working Magnet" with induction coils to convert motion into electrical energy. The magnets on both sides are the "*Impinging Magnets*".

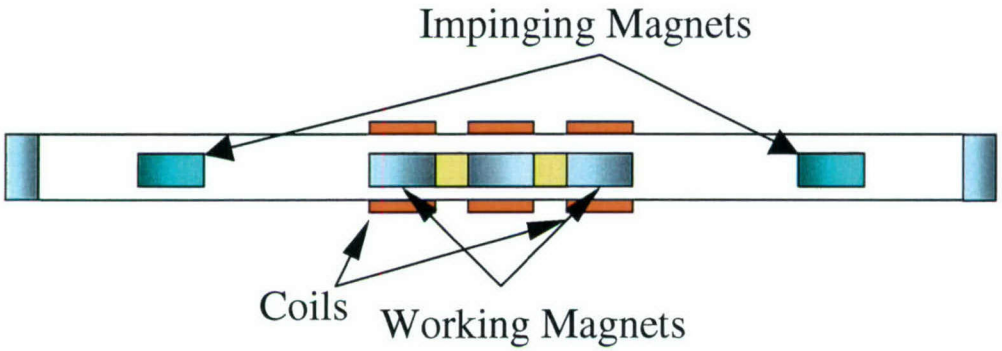

Figure 4.8: Schematic of a Closed Tube Generator with "Impinging Magnets"

The counter EMF does not restrict impinging Magnets since there are no coils in the sections where they move. They are close to the end of the tube and interact strongly with the recoil magnets to transfer the external excitation to the Working Magnets. We repeated the coupling efficiency measurements at various level of accelerations, and compared the results with the single magnet stack generator. There is an improvement over the entire acceleration range especially for low acceleration excitations where the advantage is drastic.

To demonstrate the advantage of using impinging magnets to enhance energy coupling, we compared the performance of two generators that used the same number of magnets and coils but arranged them differently so that one is a single stack generator and the other is a 3-stack generator. Generator # 1 is a single stack generator with 4 segments of 1" diameter 1.25" length magnets. Energy was harvested by three coils connected in series. 1" diameter and 0.25" thick magnets were used as recoil magnets. Generator # 2 has the same housing, except the 4 segments were divided into three parts. A 2-segment stack was at the center to serve as the "Working Magnet" and the other two magnets were used as "Impinging Magnets" with one on each side of the "Working Magnet". The three coil outputs were individually rectified and connected in parallel. These two generators were placed horizontally and oscillated by a leaf spring under the same excitation conditions with oscillating amplitude of approximately 1.4". Table 4.1 shows the output power at two different oscillating frequencies. The advantages of using impinging magnets are clear under these conditions.

Table 4.1: Output power vs oscillating frequency

	2.02 Hz	4.4 Hz
Single stack generator	0.38 W	2.06 W
Three stack generator	0.92 W	5.1 W

Although multiple stack generator with impinge magnets has a broader dynamic range with respect to efficiently coupling the horizontal axial excitation, the downside is that it requires additional generator length. One solution to this limitation is a circular multiple stack circular generator that will be discussed in Section 5.

4.1.2 Vertical rocking excitation

The second method to couple external energy into the generator is a rocking motion, which is one of the most natural movements of ocean buoys. In this mode, a magnet is moved by gravitation to slide down inside a tube during the rocking motion. The total energy available for harvesting equals the potential energy difference between the highest and the lowest positions of the magnet during rocking. Its power output depends on magnet size (i.e. total mass), tube length and inclination (i.e. height), rocking angle (i.e. acceleration), and other design factors (e.g. ferrofluid bearing properties, recoil magnet strength, coil specification, air gap dimension, and magnet stacking geometry).

Our electro-mechanical model for the linear generator together with the magnetic flux analysis software, MagNet™, are able to predict the generator performance with reasonable accuracy and give guidance to generator design and improvement.

Throughout this program, we made numerous closed tube single stack generators and tested their performance under various rocking conditions. We will present detailed results on only two generators, both of which use large magnets to produce sufficient

power to meet the program's objective. Their design specifications are tabulated in the following:

Table 4.2: Close tube single stack generators

Gen No.	Magnet segment size (FxL)	Spacer size (FxL)	Magnet material	Number of segments	Recoil magnet size (FxL)	No. of coils	No of turns and wire size	Tube dimension (FxL)
Gen 1	1.1"x1"	0.95"x0.25"	NdFeB #32	11	1x0.25	6	680 #22	1.5x24
Gen 2	1.5"x1.2"	1.5"x0.25"	NdFeB #30	8	1.5"x0.2"	12	800 #22	1.5"x26

A determination of efficiency (η_2) for converting the total potential energy loss to AC electrical energy captured in the load at various load resistance was made. The measurement is straightforward by sliding the magnet stack from one end of the tube to the other while measuring the total energy captured across various load resistors. Fig. 4.9 shows such a measurement made at 20° inclination. Energy increased with the increase of load resistance and reached a broad peak of 740 mj at 180 Ohm. The captured energy at the peak was 740 mj during the single slide. Since the total loss of potential energy during the slide was 1210 mj, the conversion efficiency is about 60%. In the range from 10° and 30°, the efficiency remains nearly constant between 58-63%.

The generator was also placed on a mechanical rocker to simulate the wave motion at 20° and various frequencies. Fig. 4.9 also plots the energy captured per slide (i.e. half of a rocking cycle) vs. load resistance for various rocking frequencies.

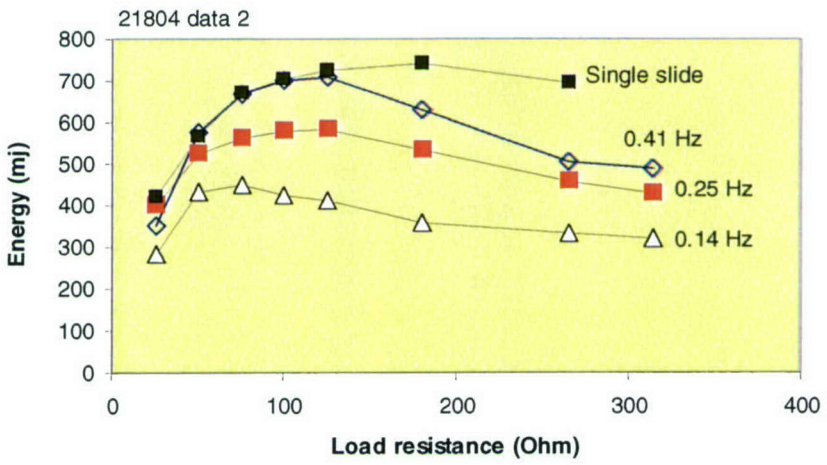

Fig. 4.9: Energy captured vs load resistance during a single slide to cover the entire length of the tube and from various rocking frequencies

They are compared to the free sliding data that represent the limit of the amount of energy that can be captured. As the load resistance becomes larger, the rocking data start to deviate from the free sliding data and the discrepancy increases with the increasing load and decreasing rocking frequency. This is caused by the lack of synchronization between the rocking movement of the sliding motion of the magnet. At low rocking frequency, the sliding velocity of the magnet was slowed down by the counter EMF. The rocking movement reversed its direction before the magnet reached the end of the tube; therefore it reduced the potential energy drop.

We also plot the data in the form of average power vs. load resistance at different rocking frequencies (Fig. 4.10). The effect of low power output due to the lack of synchronization between rocking motion and magnet sliding movement is even more prominent. There are two ways to increase the captured energy. One is to increase the generator length so the magnet has a high potential energy drop at it slides down. To illustrate this point, we lengthened the tube from 24" to 32". The result, also shown in Fig. 4.10, shows that at 0.4Hz rocking, the magnet sliding motion and the rocking motion are still in synchronization. The output power of 980 mW is nearly double that from the shorter tube, as expected. Also included in the measurement are two data points of a similar generator but with the body extended to 32" long. However, at lower rocking frequency of 0.1 Hz, the power decreased to only 220 mW. Another approach to increase the power is to use larger magnets. A generator with 1.5" diameter magnets that has been tested extensively uses 1.5" diameter magnets to generate more power. The generator has eight 1.5" diameter 1.8" length magnet segments in a 25" long tube wrapped with four coils. Under similar rocking condition to the other generator, it produces up to 1.24 watts of power. But it has the same problem at lower rocking frequency when the magnet movement and the rocking lost their synchronization. Both generators were field tested at Scripps.

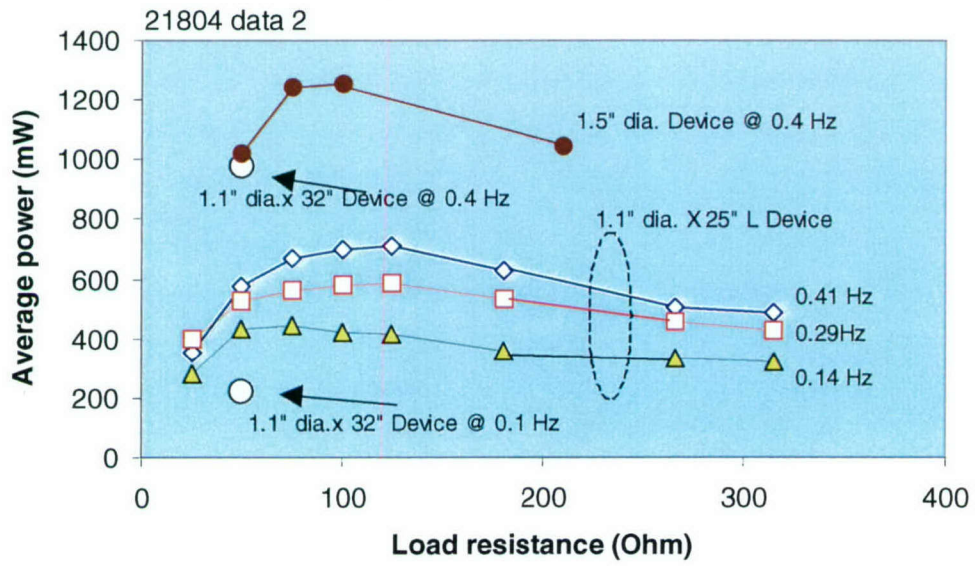

Figure 4.10: Average power vs. load resistance at different rocking frequencies of two generators (1.5" and 1.1" diameters)

Unlike the horizontal axial excitation that is in the form of pulses, excitation by rocking motion is continuous and varies sinusoidally with time. The magnitude of acceleration acting on the magnet is gSinΘ where g is gravitational constant and Θ is the rocking angle. The power output for a given generator under known rocking condition can be calculated from solving the equation of motion. Just like any other closed tube generator, external energy moves the entire system and its action on the magnet is indirect. The expression for average power output has a similar form except that the excitation is a periodical sinusoidal function. The constant "0.6" was determined empirically. The factor ϕ is a correlation factor to account for the timing of the sliding magnet and the rocking movement.

$$P_{Captured} \cong \frac{0.6\times(M_{Magnet}/M_{Total})\times\phi\times\int_{t_0}^{t_1} E_{Excitation}(t)dt}{(t_1-t_0)} \qquad (5)$$

Therefore, in order to increase the amount of captured power, one must increase the mass of the moving magnet stack with respect to the entire system; the excitation energy by buoy design, and synchronization between the magnet motion and buoy position.

4.1.3 Field Tests at the Scripps Institute of Oceanography

Both generators were field tested just off the pier of Scripps Institute of Oceanography in La Jolla, California. A Closed Tube Single Stack generator which has been thoroughly characterized and bench tested as described in the above sections was integrated to two different types of floats. These floats were designed to interact with ocean waves in different ways to create different types of excitation.

4.1.3.1 Rocking motion energy harvesting buoy

The first set up is based on a regular dock buoy. Fig. 4.11 shows the schematic of its frontal view. The float (C) is cylindrical with total buoyancy of nearly 200 lbs. The generator under test was sealed inside a 6" diameter, 28" long vinyl tube (A) secured horizontally on the top of the float. A smaller tube (B) containing an instrumentation package, including 3-axis accelerometer, rectifying circuits, timers and compact memory was placed on top of the large tube. To make the float unstable when it interacted with waves, we tethered to its top bridle a polyurethane rope on one side and tied damper plates (D) to the rope.

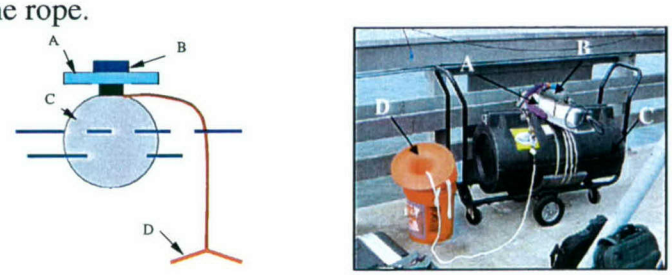

Figure 4.11: An Energy Harvesting Buoy relying on its rocking motion

As an ocean swell approaches, the float will rise with the wave but its vertical movement will be impeded asymmetrically by the damper plates bridled on one side. It will be "jerked" from that side resulting in rocking motions. This motion is confirmed by the measurement along the direction of the generator shown in Fig. 4.12. It shows the axial acceleration during one period of a 15 second swell. From the magnitude of the acceleration, we calculate the rocking angle to be between 15° to 25° at 0.5 Hz

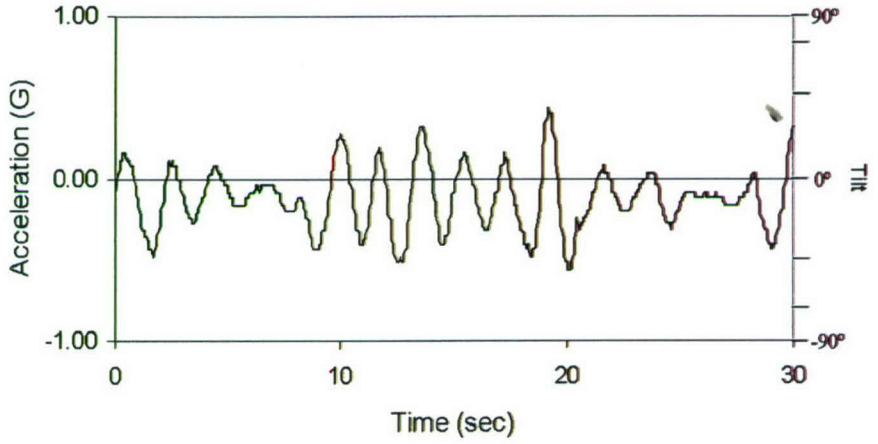

Figure 4.12: Accelerometer data to monitor rocking motion

Fig. 4.13 shows the output power spectrum during a 30 minutes period. The test was carried out just off the pier a few hundred feet from the beach. The sea was calm with a few wind chops and 15 second swells with waves of under 0.5 meter. Power output averaged over a 10 second period varied from as high as 362 mW to just a few mW. The magnitude of power output correlates with the float motion. The highest power output was achieved when the float rocks at 15° -25° angle of inclination and 0.45 Hz frequency that is slightly faster the frequency of the swells at 0.14 Hz. However, in some instances, when the wave was low, the rocking motion completely stopped. In the second design, we incorporated new designs to correct this problem.

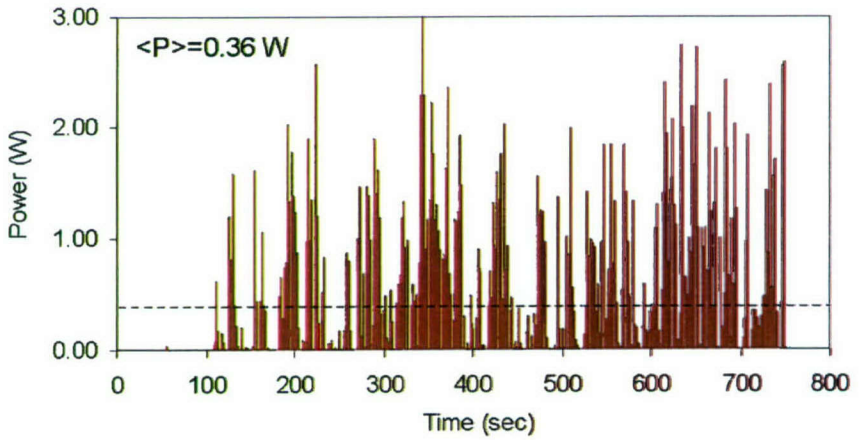

Figure 4.13: Power output from a Rocking Motion Wave Energy Harvesting Buoy

4.1.3.2 Oscillatory wave energy harvesting buoy

The second system, shown in figure 4.14, had a completely different design. The linear generator was mounted horizontally on four fiberglass stilts anchored to a large flat floating plate. The plate is connected to smaller satellite floats via long fiberglass rods on four sides for additional buoyancy.

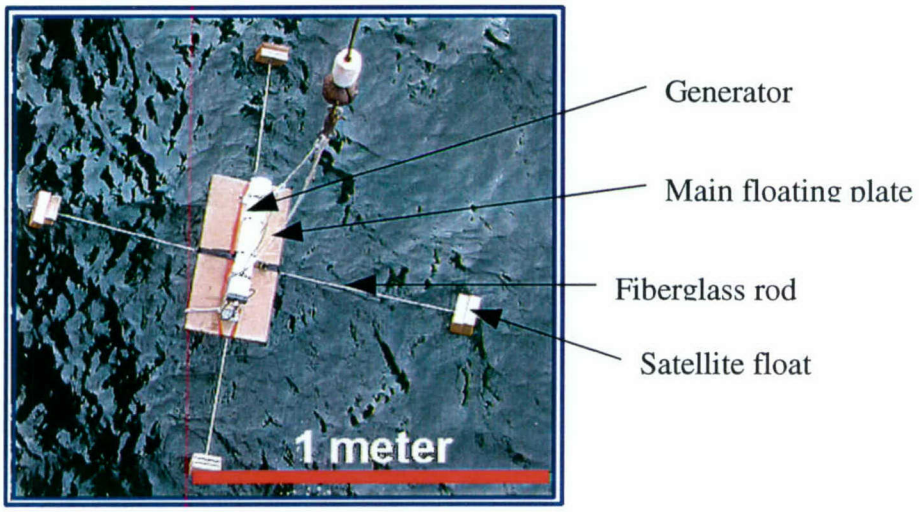

Figure 4.14: Top view of an Oscillatory Wave Energy Harvesting Buoy with fiber glass rods and small satellite floats.

This system has a large footprint defined by the area covered for the satellite floats. Wave energy from this area can be collected and stored in the fiberglass rods and stilts as elastic energy that can be constantly release to cause the generator to oscillate at high frequency. The was verified by measuring the axial acceleration of the generator. The oscillatory movements, shown in figure 4.15, was present even between large swells and the frequency was about one magnitude larger that the swells.

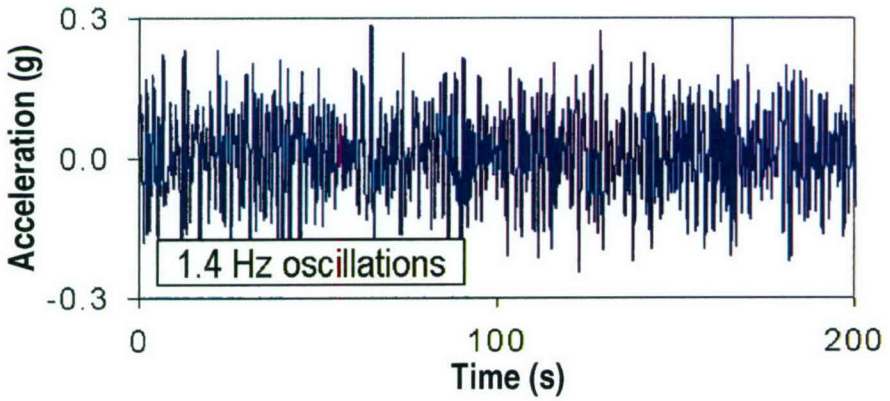

Figure 4.15: Lateral oscillations of the generator

Consequently, this system delivered power output continuously without any "quiet" period even in calm ocean condition. Results are shown in figure 4.16.

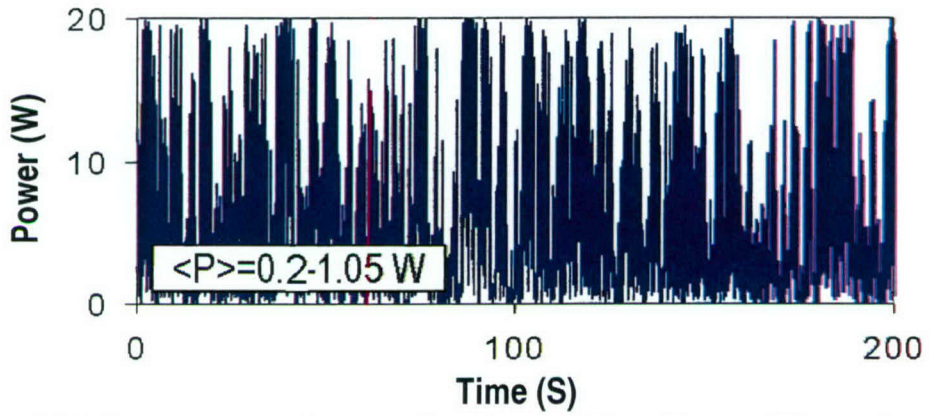

Figure 4.16: Power output form an Oscillatory Wave Energy Harvesting Buoy

4.1.4 Long-term operation reliability and stability test

We tested the long-term performance of a Closed Tube Single Stack generator on a mechanical rocker. The generator with a 14" long, 1.5" diameter single stack placed in a 34" long tube with 4 sets of induction coils was rocked at 20° at 0.4 Hz continuous for 2 weeks. The outputs from each coil were rectified, controlled and regulated to be combined into a single output to charge a Pb-acid battery. We achieved an average output of 1.82 Watts throughout the test. This study, shown in Fig. 4.17, demonstrated the stability of generator operation under high load condition.

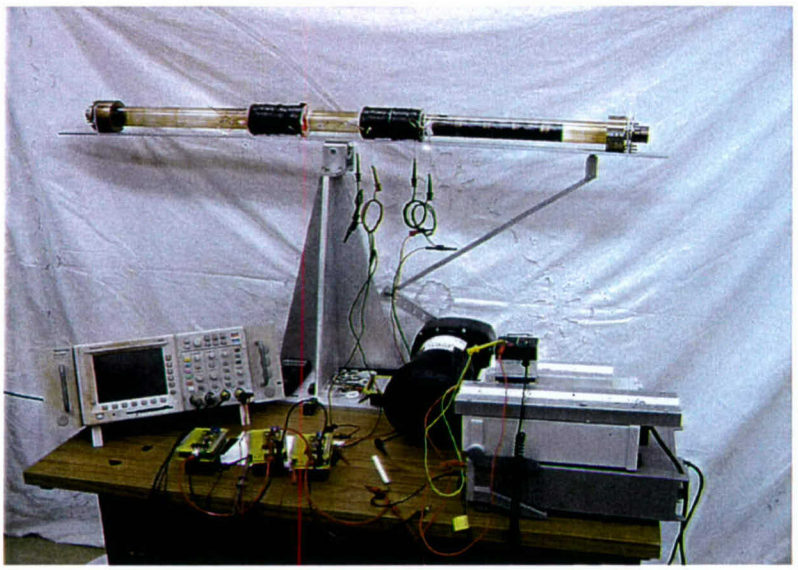

Figure 4.17: Long-term operational stability and reliability test setup

4.1.5 Limitation of Closed Tube Generator

Our studies have successfully shown that the Closed Tube Generators can harvest energy from ocean waves despite their simplicity. However, after some detailed analysis, we also point out the most significant limitation - the inefficient energy coupling from external excitation (e.g. waves) to internal motion of the magnet. The energy transfer is indirect so that a large portion of the excitation is wasted in moving the entire system without producing significant relative movement between the coils and the magnets. The situation can be improved by multiple magnet generators to broaden the dynamic range for coupling sensitivity or by a circular generator to remove the end effect and ease the difficulty in synchronizing the rocking and magnet movements. Another radical approach to improve performance is the Semi-Closed Tube Generator in which the external excitation can be coupled into the magnet directly.

4-2 Semi-closed Tube Generator

In a semi-closed tube generator, the magnet can be accessed directly via a point absorber which is a generic term often used in Ocean Wave Conversion technology to describe a device component to focus the wave energy and directly transfer it into the system. They come in different sizes and shapes. In the Semi-Closed Tube Generator that we have developed, the design is very simple (Fig. 4.18). Basically, it shares the same features as a Closed-Tube Generator described in the previous sections, except the magnet stack connects to a center shaft with a large area paddle on the other end. One end of the tube is sealed with a bellow, so the magnet can be moved by pushing or pulling the point absorber. Since ferrofluid bearing is used, the generator can operate in any orientation.

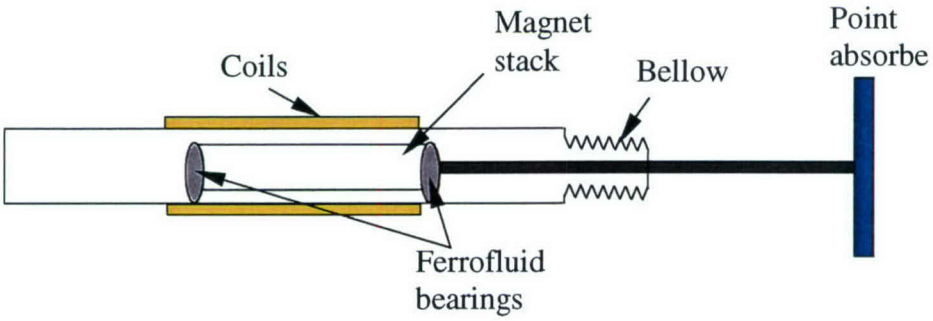

Figure 4.18: A wave energy generator with a point absorber generator

We tested two of these type of generators. Generator #3 shares the same basic design as the Closed Tube Single Stack generator #1. Generator #4 shares the same design as closed tube Single Stack Generator #2. The point absorber is a 6" diameter aluminum plate. They were characterized with two types of external excitation, a pulsed excitation similar to conditions used to characterize the Closed Tube Generator, and continuous linear movement at different velocities. Measurements were made at both horizontal and vertical orientation.

4.2.1 Pulsed excitation

Energy output from the generator due to pulse excitation was measured in a horizontal position. Measurements were made by attaching the point absorber to a calibrated leaf spring and varying the load resistance. The conditions were the same as those used to characterize the closed tube single stack generator characterization (i.e. 2.4 m/sec^2 initial acceleration and 1.12 Joule total energy/pulse). Results are shown in Figure 4.19.

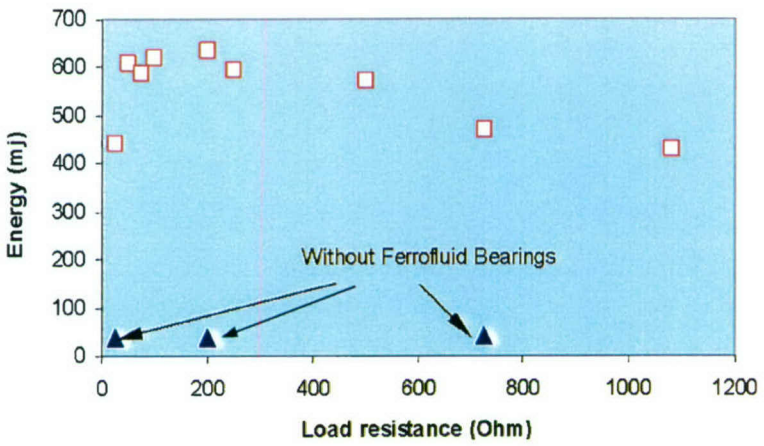

Figure 4.19: Energy output vs. load resistance from a Closed Tube Generator with a Point absorber under pulsed excitation

The peak energy output is about 650 mj, which is larger than the energy produced by the Closed Tube Generator under the same direct excitation (see figure 4.6). This would correspond to the combined conversion efficiency (η_1 x η_2) of approximately 58%. The external excitation is directly coupled to the magnet to generate differential movement between the magnet and the generator. *Without ferrofluid bearings, the generator is very inefficient since the magnet stack is too heavy for the excitation to overcome.*

4.2.2 Continuous linear movement

The major advantage of a semi-closed generator with point absorber is its response to slow yet powerful continuous linear movement such as ocean waves. The excitation is direct to create a differential between the coils and the magnets. We excited the generator by moving the point absorber back and forth over a distance of 6 inches at different velocities. Results are at three different load resistances are shown in Fig. 4.20. The dependence is linear on the square of velocity as expected from the relationship $E=V^2/R_{Load}$. Because the external force creates a differential movement between the magnets and the coils directly, very little energy is wasted to move the entire device. As a matter of fact, additional mass to the rest of the generator will make the system more immobile, thus favoring the power harvesting process. One approach to integrate this device to a buoy is to place it in a horizontal position with the point absorber pointing toward the rocking direction. The area of the point absorber should be large to absorb the external excitation and focus it to move the magnet stack. It should be made of highly buoyant material, so as the buoy rolls and rocks, the pointer will hit the water. The powerful yet slow force will push the point absorber effectively to generate sizable power output.

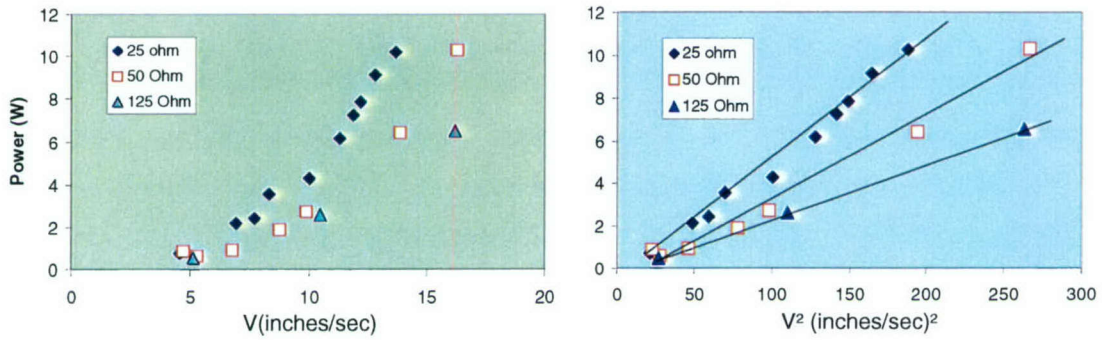

Figure 4.20: Power out put vs. velocity of the point absorber movement for three load resistors. 1.5" diameter, 1.2" L magnets

Another approach is to operate the device vertically. Extensive tests were made on a generator with 1.106" diameter, 1.25"L magnets and matching coils connected to a 55 Ohm load resistor. This generator uses magnet stack about one-half the size of the generator used for horizontal operation (see figure 4.20). Its output power dependence of the vertical velocity of the magnet stack is shown in Fig. 4.21. A buoy with reasonable size of a few hundred pounds of buoyancy will be able to drive a multiple number of these generators.

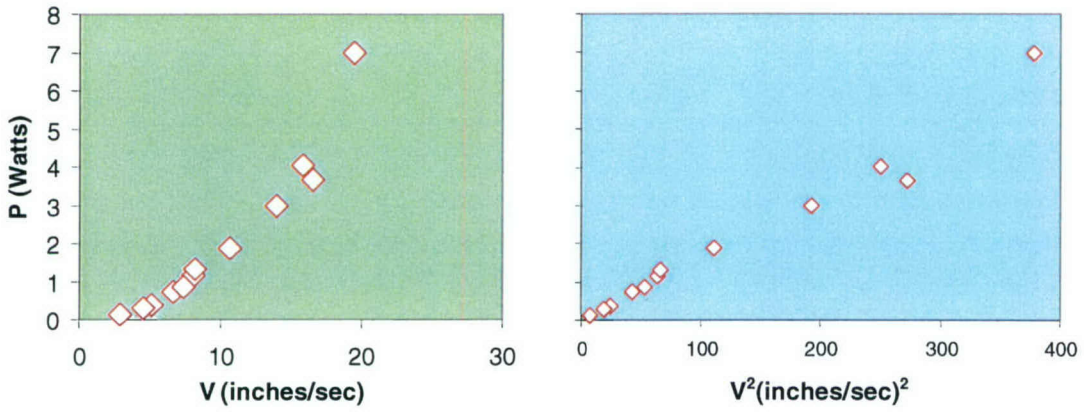

Figure 4.21: Power output of a vertical device with 1.162" diameter magnets

5.0 Future Plans

(Adaptive Wave Energy Harvester)

The net efficiency for converting ocean wave energy to regulated electricity is the combined efficiency of three processes: coupling of external energy into the generator, converting motion of the magnet into random electrical energy and finally into regulated DC output. Through the current program, we have accomplished the development and understanding of the second and the third process and shown their combined efficiency to be approximately 60% x 80% = 50%. The next challenge is to improve the efficiency of the first process, not through design improvement on what we have already done, but through the design of more interactive buoys. We propose an **Adaptive Wave Energy Harvester** with re-configurable mechanical form as well electronic circuitry to maximize its interaction with wave motion under a wide range of sea states. The approach is depicted in the following flow diagram.

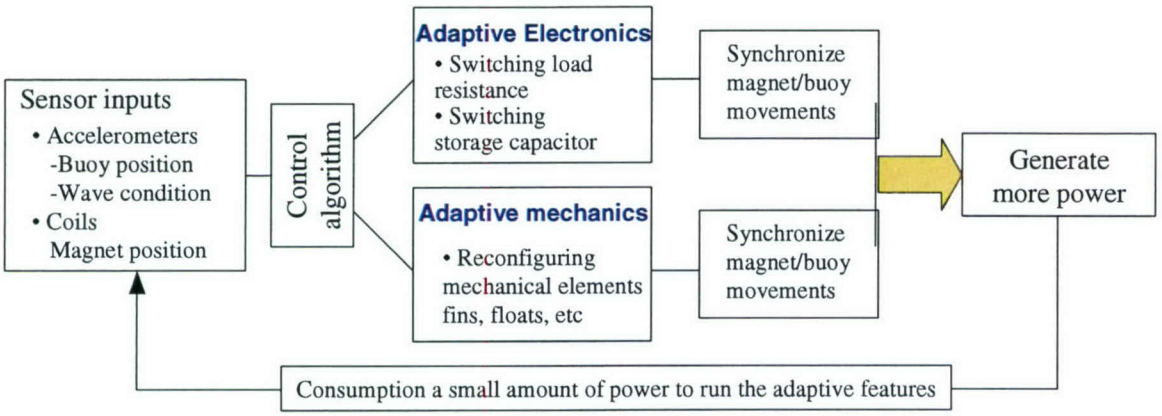

Figure 5.1: Flow Chart of an Adaptive System

The "Smart System" is equipped with accelerometers to monitor the float position and wave conditions. The induction coils serve a dual function to harvest energy and monitor position of the magnets. These inputs will trigger a decision algorithm to reconfigure electronic circuits and mechanical structures in real time.

Re-configurable Electronic Circuits include switching capacitors and changing load resistance in real time to control the slow-down or speed-up the magnet movement via its interaction with counter EMF, such that it will be synchronized with the buoy movement.

Re-configurable Mechanical Structures include actuation of simple mechanical elements such as fins and floating plates. Their deployment and retrieval will be synchronized with wave motion to maximize the interaction between the float and the waves. As a result of the adaptive features, more power can be generated and a small fraction of that will be used to operate the buoy reconfiguration. We propose two classes of generator configurations as development platforms: an Indirect Interaction Device and a Direct Interaction Device.

5-1 Indirect Interactive Harvester (Orthogonal Circular Device)

The orthogonal circular generator is a closed-tube multiple stack generator in which magnets are placed inside a circular tube with their magnetic axes perpendicular to the motion (Fig. 5.2a). Magnets are aligned with alternate polarity and fixed on a spacer that matches the curvature of the circular generator body. Multiple stacks can be placed in the circular body with the polarity of the end magnets of each stack being the same such that two stacks will repulse each other as they approach. In this configuration, the ferrofluid cushion engulfs the entire end area of the magnet and can support a heavy load while maintaining the ultra low friction characteristics (Fig. 5.2b). In addition, the circular design eliminates end effects associated with linear devices. A magnetic bridge filled with a higher-grade ferrofluid (μ=100) connects the top and bottom sides shown in Fig. 5.3 to complete the magnetic circuit. Coils are placed around the magnetic bridge to capture flux and generate energy as the magnet stack slide across.

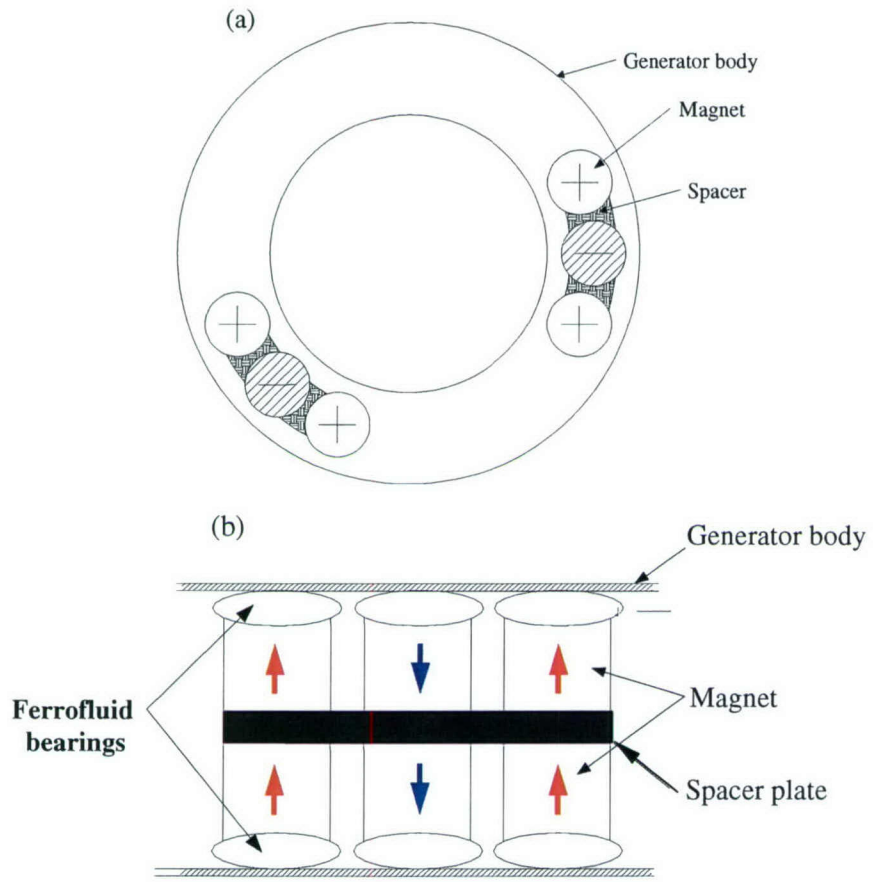

Figure 5.2: (a) Top view of a circular orthogonal device
(b) Side view of a circular orthogonal device

In this configuration, the ferrofluid functions not just as an ultra low friction lubricant but also provides a low magnetic reluctance path to direct flux through the bridge. Figure 5.3 shows a model calculation of magnetic flux distributions in a traditional configuration where the magnetic axis is parallel to the direction of the movement and the orthogonal configuration with a magnetic bridge. The use of ferrofluid cushion and magnetic bridge to direct the flux nearly eliminates the flux leakage in the air gap and at the end of the magnet. By advancing the magnet stack the length of a single magnet, the net change in magnetic flux in the coils is 2.7 times greater than in the parallel configuration. Since the energy captured is proportional to the square of the rate of flux change, the total amount of captured energy by the orthogonal configuration will be 7 times more if the magnet stack moves through the coil at the same velocity.

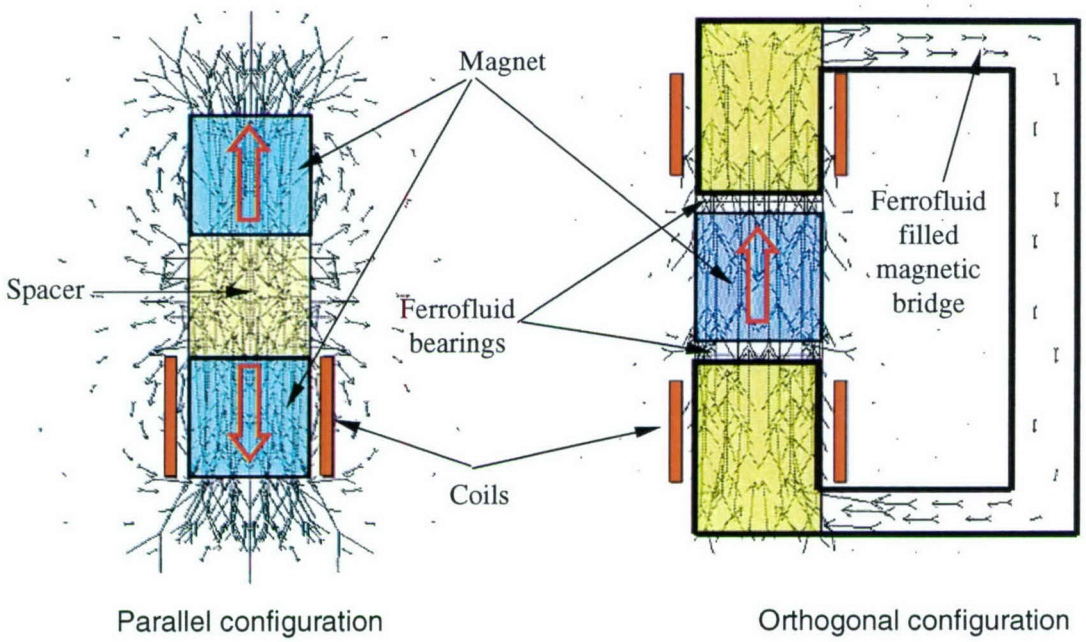

Figure 5.3: Magnet flux analysis in Parallel and Orthogonal configuration. Notice the fringe field loss is greatly reduced in the orthogonal configuration.

The circular orthogonal generator device is relatively simple and very robust. All moving parts can be permanently sealed to protect them from the severe marine environment. However, the interaction between the magnet and ocean waves is indirect therefore only a small fraction of energy is petitioned into moving the magnet. In order to increase the power generation, direct access to the magnet stack will be needed to couple with the external excitation.

5-2 Direct interactive devices (Generator with a Point Absorber)

The use of a point absorber separates the motion of the magnet stack from the rest of the system, thus increasing the coupling efficiency of the wave energy. We consider two examples: direct interactive devices relying on rolling motion (i.e. lateral yaw) and heave motion (i.e. up and down vertical motion).

5.2.1 Harvesting energy from the rolling motion of a buoy (lateral yaw)

A surface wave-riding buoy can be used as the test platform to capture the energy associated with rolling motion. Figure 5.4 shows a schematic design. A multiple segment magnet stack with a point absorber floating plate is inserted into a hollow shaft near the bottom of the buoy at an angle. Coils are wrapped around the shaft housing inside the buoy to complete the generator. It will be best for the generator to have the orthogonal linear design because of the very strong counter EMF it produces, thus making it suitable to harvest energy from the slow yet powerful wave movements. Figure 5.5 shows the harvester in action sequence. As the buoy rolls (Step 1), accelerometers inside the buoy will sense the motion and send a signal to switch the coils on the opposite side (i.e. Idle Generator) to a large load resistor. Consequently, the counter EMF will decrease and the magnet stack will slide down freely due to the ultra low friction ferrofluid bearings (Step 2). After completing the roll, the buoy reverses its direction (Step 3). The action is again sensed by accelerometers to trigger the same coil to an impedance matching load resistor and to transform it from an "Idle Generator" to an "Active Generator" (Step 4). The coil will generate strong counter EMF and capture a large amount of energy as the rolling motion of the buoy pushes it over the magnet stack resting on the floating point absorber. The process repeats itself with each wave. Multiple generators can be mounted around the buoy to capture rolling motion in all directions.

Re-configurable mechanical elements can also be actuated and retrieved in synchronization with wave movement to further enhance their interactions. Because of the direct interaction with wave energy, the coupling of external energy into the device is much more efficient than the Indirect Interactive Devices.

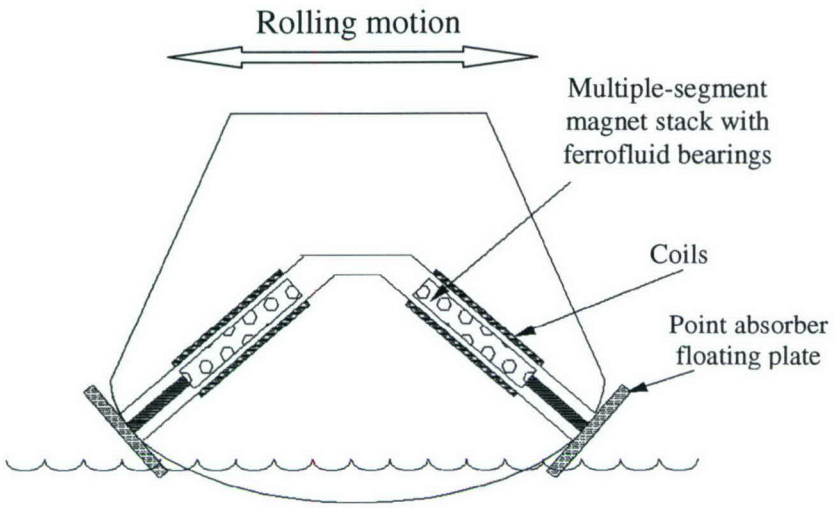

Figure 5.4: Energy harvester with point absorber on a surface wave-riding buoy

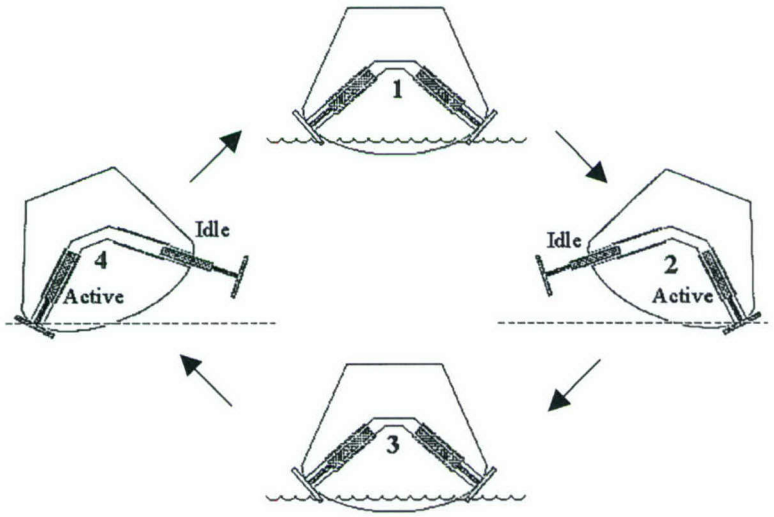

Figure 5.5: Adaptive Ocean Wave Energy Harvester in action

5.2.2 Harvesting energy from the heaving motion of a buoy (vertical rise and fall)

Figure 5.6 shows a device operating in vertical position. The main buoy is a long tube with hollow shaft(s). Coils are inside the float around the shaft housing. The magnet stack(s) is attached to a large damper plate made of high buoyancy material such that the magnet stack assembly is nearly density neutral. The shape of the vertical cross section of the buoy can be specially designed so the buoy interacts with the wave motion non-linearly and converts the slow motion to vertical heave (i.e. vertical rise and fall) at higher frequency, thus broadening its operational dynamics to a wide range of sea states.

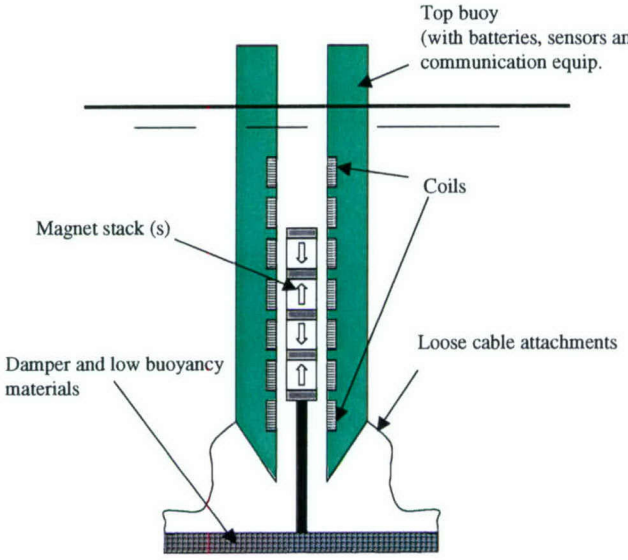

Figure 5.6 Vertical device

Table 5.1 calculates the total available power in the heave motion of a cylindrical buoy of various sizes in a range of sea states. It points out the potential of the vertical device.

Table 5.1

SEA STATE				Size	Performance		
Sea State	Wind (kts)	Wave (ft)	Period (sec)	Diameter (m)	Energy (J)	Power (W)	Power (W) 10%
1	5	1.0	2.0	0.2	28.6	14.3	1.4
2	10	2.0	3.0	0.2	114.4	38.1	3.8
3	15	4.0	4.0	0.2	457.4	114.4	11.4
4	19	7.0	5.0	0.2	1400.8	280.2	28.0
5	23	10.0	6.0	0.2	2858.8	476.5	47.6
6	31	18.0	8.5	0.2	9262.6	1089.7	109.0
7	40	30.0	11.0	0.2	25729.3	2339.0	233.9
4		7.0	5.0	0.2	1400.8	280.2	28.0
4		7.0	5.0	0.3	3151.8	630.4	63.0
4		7.0	5.0	0.5	8755.1	1751.0	175.1
4		7.0	5.0	1	35020.5	7004.1	700.4

1 knot = 1.1508 Miles/Hour

6.0 Comparison with Other Renewable Energy Sources

6-1 Solar Power

Radiant power from the sun, to most of the populated earth surface, after atmospheric reflection and absorption, averages 644 Watts per square meter. It is available for 5-8 hours on stationary photovoltaic panels, installed to receive maximum sunlight. By assuming 10% conversion efficiency, this will correspond to 64 watts for 5-8 hours per day or average to 13-21 watts for a 24-hour period. This upper bound value assumes the panels are stationary under optimum conditions at all time. However, in the marine environment, water conditions, salt precipitation or interference by marine life can have a drastic effect on conversion efficiency. For this reason, solar panels on ocean-bound buoys are all mounted in a near vertical opposition. In addition to variation in weather and seasonal conditions, the latitude of deployment affects solar panel performance. Finally, solar panels are large, and thus require a large buoy as a support base. The above-surface structure is large and very visible.

6-2 Wind Power

There are no commercial buoys equipped with windmills other than a few custom designed units where the manufacturer offers to retrofit senor buoys with mini-wind turbines used on sail boats. Their turbines weigh close to 100 lbs with a tip-to-tip distance of 2 ft. Power generation can be estimated from the following formula:

$$\text{Power (Watts)} = (0.0049) \times (\text{Wind speed in miles/hr})^3 \times (\text{Swept area in square feet}) \times (\text{Efficiency\%})$$

Assuming a turbine efficiency of 40%, then the power output of the above unit for wind velocity between 10-20 miles/hours are:

Wind velocity (mph)	Power (w)
10	6
15	20
20	50

Overall, wind energy is not a popular choice among oceanographers. The major concerns are intermittent operation, drift, and survivability in severe weather condition. In addition, just as with the solar panel, windmills require a large buoy base and are very visible.

7.0 Summary

Through this program, we have developed a new class of ocean wave energy harvesters that are modular, robust and small enough that they are easily deployable or can be retrofitted to existing buoys. The principle of operation is very simple, based on existing physics of passing a set of magnets through coils to generate electrical energy. The use of a ferrofluid bearing with ultra low friction has improved the performance of these generators to a level higher than can be achieved by traditional means. Ferrofluid bearings reduce frictional loss and frictional wear, and at the same time enhance the system's sensitivity to interact with the random motion of ocean waves for energy capture. Unlike solar and wind-powered buoys, buoys with this generator can have a low profile and will not be easily visible. Work performed during the program can be divided into two parts:

- Basic studies: Ferrofluid bearings properties and improvement, generator design and modeling
- Applied studies: Generator fabrication and testing.

We have developed two classes of generators. The first type of generator has a closed tube configuration completely sealed against the hostile ocean environment. When it is integrated with a 200 lb buoyancy dock buoy in a low sea state condition, it can generate close to 1 Watt of continuous power. Although the efficiency for converting magnetic motion energy to regulated DC power is about 50%, its efficiency for coupling wave energy into the system is very low due to the indirect coupling mechanism. However, its simplicity and low cost make it an attractive energy harvesting system for low power applications. We propose that an adaptive buoy with a circular generator design will improve its performance.

The second type of generator is a semi-closed tube with a point absorber to couple the magnet to the external excitation directly. The coupling efficiency is much higher even for the slow yet powerful type of excitation. This type generator with the same size as the closed tube generator can produce up to 10 watts of power for the point absorber velocity to be 15 inches/sec or lower. If an adaptive buoy can be developed with this generator, we expect power production in the range of 10-100 W to be possible.

Finally, we have successfully field-tested two types of wave energy harvesting systems: Rocking Motion Wave Energy Harvesting Buoy and Oscillatory Wave Energy Harvesting Buoy. The latter is a very promising design. It can deliver continuous power even in calm ocean condition.